Distinguishing the combined vegetation and soil component of $\delta^{13}C$ variation in speleothem records from subsequent degassing and prior calcite precipitation effects

Heather M. Stoll[1*], Chris Day[2], Franziska Lechleitner[3], Oliver Kost[1], Laura Endres[1], Jakub Sliwinski[1], Carlos Pérez-Mejías[4], Hai Cheng[4], Denis Scholz[5]

[1]Department of Earth Sciences, ETH Zurich, Sonneggstrasse 5, 8006 Zürich, Switzerland
[2]Department of Earth Sciences, University of Oxford, South Parks Road, OX1 3AN Oxford, UK
[3]Department of Chemistry and Biochemistry & Oeschger Centre for Climate Change Research, University of Bern, Freiestrasse 3, 3012 Bern, Switzerland
[4] Institute of Global Environmental Change, Xi'an Jiaotong University, Xi'an, China
[5] Institute of Geosciences, University of Mainz, Mainz, Germany

Correspondence to: Heather M. Stoll (heather.stoll@erdw.ethz.ch)

Abstract.

The carbon isotopic signature inherited from soil/epikarst processes may be modified by degassing and prior calcite precipitation (PCP) before its imprint on speleothem calcite. Despite laboratory demonstration of PCP effects on carbon isotopes and increasingly sophisticated models of the governing processes, to date, there has been limited effort to deconvolve the dual PCP and soil/epikarst components in measured speleothem isotopic time series. In this contribution, we explore the feasibility, advantages, and disadvantages of using trace element ratios and $\delta^{44}Ca$ to remove the overprinting effect of PCP on measured $\delta^{13}C$ to infer the temporal variations in the initial $\delta^{13}C$ of dripwater prior to degassing and PCP. In 98 examined stalagmites, the most widely utilized PCP indicators Mg/Ca and $\delta^{44}Ca$ covary as expected. However, Sr/Ca does not show consistent relationships with $\delta^{44}Ca$ so PCP is not ~~universally~~ the dominant control on Sr/Ca. From $\delta^{44}Ca$ and Mg/Ca, our calculation of PCP as f_{Ca}, fraction of initial Ca remaining in solution at the time the stalagmite layer is ~~at the deposition of the stalagmite layer~~deposited, yields multiple viable solutions depending on the assumed $\delta^{44}Ca$ fractionation factor and inferred variation in D_{Mg}. Uncertainty in the effective fractionation of $\delta^{13}C$ during degassing and precipitation contributes to uncertainty in the absolute value of estimated initial $\delta^{13}C$. Nonetheless, the trends in initial $\delta^{13}C$ are less sensitive to these uncertainties. In coeval stalagmites from the same cave spanning the 94 to 82 ka interval, trends in calculated initial $\delta^{13}C$ are more similar than those in measured $\delta^{13}C$, and reveal a common positive anomaly initial $\delta^{13}C$ during a stadial cooling event. During deglaciations, calculated initial $\delta^{13}C$ implies ~~the~~a trend of greater respiration rates and higher soil CO_2 ~~is captured in the calculated initial $\delta^{13}C$~~, although the higher interglacial dripwater saturation ~~despite the tendency of higher interglacial dripwater situation to~~ favors more extensive PCP. Initial $\delta^{13}C$ can be estimated for active and fossil ~~speleothems~~ from a range

of settings, wherever there is confidence that Mg/Ca and/or $\delta^{44}Ca$ provides quantitative indication of past changes in PCP. Further study of Mg partitioning in speleothems will improve the robustness of Mg/Ca as a PCP proxy.

1 Introduction

~~In the mid- and high latitudes, c~~Changes in vegetation productivity and soil processes significantly influence the $\delta^{13}C$ of dripwater. ~~The~~ $\delta^{13}C$ of CO_2 in the soil and karst reflects the relative contributions of isotopically light respired CO_2 and isotopically heavier atmospheric CO_2. Conditions which favor higher vegetation productivity, including deeper rooted trees (Meyer et al., 2014), and faster rates of heterotropic and autotrophic respiration in soils will lead to higher soil pCO_2 and a lower $\delta^{13}C$ of CO_2. In contrast, in ~~compared with~~ less productive and slower respiring systems, ~~where~~ the atmospheric CO_2 and its higher $\delta^{13}C$ will be more significant C sources in the soil. This soil and vegetation signature imparted to the dripwater is also imprinted on speleothem $\delta^{13}C$. In the temperature range characterizing the mid- and high latitudes, respiration rates and vegetation density are highly sensitive to temperature, and speleothem $\delta^{13}C$ ~~The climate sensitivity of these processes~~ has been exploited to serve as a temperature proxy in mid-latitude speleothems(Genty et al., 2006; Genty et al., 2003). Sufficient soil moisture is also required for high soil CO_2(Romero-Mujalli et al., 2019). In addition to its direct effect on the $\delta^{13}C$ of soil CO_2, higher soil CO_2 concentrations also lead to more open system dissolution of karst hostrock carbonate, which further contributes to lower $\delta^{13}C$ of the dripwater DIC.

Superimposed on soil and karst process are~~,~~ in-cave processes which subsequently modify the $\delta^{13}C$ of DIC and thereby speleothem $\delta^{13}C$, ~~since~~ ~~as~~ coupled degassing and precipitation of $CaCO_3$ progressively enriches the $\delta^{13}C$ of the remaining dissolved inorganic carbon. This process has been demonstrated in lab experiments(Polag et al., 2010; Hansen et al., 2019) and in "farmed calcite" in cave environments(Mickler et al., 2004; Mickler et al., 2006) and can be modeled as a Rayleigh process. Extensive quantitative modeling of this processes has been conducted in purpose built models (Mühlinghaus et al., 2009, 2007; Scholz et al., 2009; Sade et al., 2022) and embedded in broader models (Owen et al., 2018). Our interest here is to extend the previous analysis by relating the evolution of the $\delta^{13}C$ of bicarbonate to the evolution of the Ca in solution. In this way, we can evaluate the viability of using trace element and Ca isotopic data as independent indices of the progression of coupled CO_2 degassing and PCP.

In this contribution, we explore the potential and limitations of simple, easy to use approaches to distinguish temporal variations in $\delta^{13}C$ attributable to soil/epikarst vs in-cave processes. We acknowledge that effects to recover the absolute initial $\delta^{13}C$ will be challenging in most applications. Therefore we focus on the simpler goal of separating the temporal trends in PCP from those due to soil/epikarst components within a given stalagmite. We present new analyses of PCP proxies $\delta^{44}Ca$ and Mg/Ca on ~~9~~8 stalagmites from a single cave system which experienced the same climate regime and represent a range of climate states from glacial through interglacial. Using these stalagmites as examples, ~~and~~we evaluate approaches for

Formatted: Subscript

Formatted: Subscript

Formatted: Subscript

Formatted: Not Superscript/ Subscript

estimating the quantitative extent of PCP and degassing in fossil stalagmites in which initial dripwater chemistry and partition~~ing~~ coefficients are not independently constrained. For three time intervals including TII, MIS5b-c, and the last deglaciation, we present $\delta^{13}C$ time series , and compare trends of coeval $\delta^{13}C$ records with and without deconvolution of in cave and soil/epikarst processes.

2. 2. Background on evolution of $\delta^{13}C$ with progressive CO_2 degassing and PCP

2.1 Rayleigh fractionation of carbon isotopes during CO_2 degassing and prior calcite precipitation

The $\delta^{13}C$ value of dissolved inorganic carbon in dripwater, dominantly bicarbonate, will evolve with the coupled precipitation of calcite and evolution of CO_2 (g) from the dripwater. Because the C removed by CO_2 degassing is isotopically much lighter than the bicarbonate pool, the $\delta^{13}C$ value of the dissolved bicarbonate increases. The net total fractionation, ε_{tot} is the weighted sum mean (by the number of C atoms) of the effective individual fractionations factors (ε) between bicarbonate and CO_2 (g) and between calcite and bicarbonate, respectively(Scholz et al., 2009): ~~(e.g., Scholz et al., 2009):~~

(1) $^{13}\varepsilon_{CO2g/CaCO3(s)tot} = ½\ ^{13}\varepsilon_{CO2(g)/HCO3-} + ½\ ^{13}\varepsilon_{CaCO3(s)/HCO3-)}$

The first of these fractionations factors is strongly temperature dependent. The second, bicarbonate-calcite fractionation factor showed negligible temperature dependence in seeded experiments (Romanek et al., 1992) but modest temperature dependence in earlier studies and which were used in compilations (Emrich et al., 1970; Rubinson and Clayton, 1969; Mook and Rozanski, 2000). Thus, the net fractionation factor evolves from -3.5‰ at 25°C to -5.2‰ at 5°C using temperature-sensitive calcite fractionation factors, but from -3.5‰ at 25°C to -4.6‰ at 5°C when the calcite fractionation factor is invariant. The evolution of the $\delta^{13}C$ of the bicarbonate in dripwater has been modeled by a Rayleigh process, in which the dependence of the $\delta^{13}C$ of bicarbonate is a function of the remaining HCO3- in solution. (Mühlinghaus et al., 2009, 2007). Newer models have added the effect of isotopic exchange between cave air and the dripwater (Hansen et al., 2017). Finally, advection-diffusion-reaction models simulate the dynamic speleothem formation from a flowing thin film, including the evolution from degassing, precipitation, and exchange with atmosphere (Sade et al., 2022). This latter model confirms that that the evolution of $\delta^{13}C$ of speleothem calcite is very closely correlated to the extent of PCP once >20% of initial DIC has precipitated ~~(Sade et al., 2022)~~. Previous modeling has focused on the evolution of $\delta^{13}C$ bicarbonate as a function of the remaining DIC. In contrast, here we focus on the evolution of $\delta^{13}C$ bicarbonate as a function of the Ca remaining in the solution. The Ca remaining in solution allows us to estimate the extent of calcite precipitation, and from this we estimate the degree of degassing (and carbonate precipitation) the solution has undergone prior to deposition of the speleothem. We target Ca as the indicator because ~~because~~ ttrace element ratios and Ca isotopic systems may prec~~on~~serve proxy information about the Ca remaining in solution. ~~This effectively gives us a tracer from which we can estimate the degree of degassing and carbonate precipitation the solution has undergone prior to deposition of the speleothem.~~ CaveCalc (Owen et al., 2018) simulates this process and examples are given

Formatted: Font: Symbol
Formatted: Subscript

in Figure 1a. We therefore relate the Rayleigh-driven progressive enrichment in $\delta^{13}C$ of bicarbonate with the progressive depletion of Ca in the dripwater. fCa is the fraction of initial Ca remaining in solution. This relationship is:

$$(2)\delta^{13}C_{init} = \delta^{13}C_{meas} - A \cdot ln(fCa)$$

in which $\delta^{13}C_{init}$ is the composition for a case of negligible degassing and $CaCO_3$ ~~Ca~~ precipitation (f_{Ca} =1), and $\delta^{13}C_{meas}$ corresponds to the $\delta^{13}C$ at a given value of fCa (Table 1 provides a summary of abbreviations used in this paper). The term A describes the rate of evolution of $\delta^{13}C$ with progressive degassing and $CaCO_3$ precipitation. We subsequently refer to term A as the degassing slope. A range of values have been proposed for A, from ~~and explore the implications of a range of values, from the slope for~~ equilibrium precipitation and degassing in CaveCalc, to greater, kinetically-enhanced fractionation during degassing suggested by some laboratory(Hansen et al., 2019) and field (Mickler et al., 2019) studies (Figure 1b; Supplemental Figure 1). The support for each of these values and implications are discussed at length in section 5.3. To test the influence of different degassing slopes on the magnitude of the PCP effect, we complete a sensitivity analysis with a range of values for the parameter A.

Formatted: Subscript

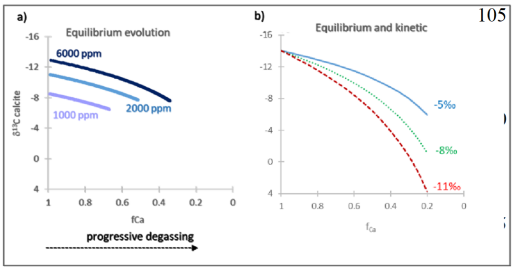

Figure 1. a) Simulation of the equilibrium evolution of $\delta^{13}C$ in calcite with increasing PCP for three initial $\delta^{13}C$ of DIC corresponding to different pCO_2 of soil, with the soil CO_2 isotopic composition following typical Keeling line (e.g. (Pataki et al., 2003). Calculations completed in CaveCalc (Owen et al., 2018). The fraction of initial Ca remaining at the time of speleothem deposition (f_{Ca}) is the index of PCP. b) Example simulation of the evolution of $\delta^{13}C$ in calcite from a single initial $\delta^{13}C$ of DIC following Equation (3); an equilibrium degassing and precipitation fractionation slope A (-5 ‰) is contrasted with two possible kinetically-enhanced fractionation slopes (-8 ‰ and -11 ‰).

Table 1. List of variables and abbreviations

Variable	Description
A	degassing slope from Eqn. 2
$\delta^{13}C$ meas	measured stalagmite $\delta^{13}C$ for a given sample
$\delta^{13}C$ init	$\delta^{13}C$ expected in stalagmite prior to degassing and PCP as calculated by Eqn. 2
$\delta^{13}C\_DIC\_init$	$\delta^{13}C$ expected in dripwater prior to degassing and PCP
fCa	modeled fraction of the initial Ca remaining at the time of speleothem carbonate deposition
fCa_δCa	proportion of Ca remaining in solution determined using calcium isotope measurements on the stalagmite
fCa_MgCa	proportion of Ca remaining in solution determined using Mg/Ca measurements on the stalagmite
fCa (fit)	proportion of Ca remaining in solution, calculated from Mg/Ca measurements on the stalagmite with adjustments for compatibility with fCa_δCa
fCa^{o}	fCa_MgCa with AF=1 and B=1
B	scaling factor to estimate bedrock Mg/Ca from minimum stalagmite measured Mg/Ca, as in Eqn. 6
AF	attenuation factor to transform fCa_MgCa into fCa(fit) as in Eqn. 7
Mg/Ca initial	inferred bedrock Mg/Ca and initial dripwater Mg/Ca
Mg/Ca min	minimum Mg/Ca measured in a given stalagmite
Mg/Ca meas	measured stalagmite Mg/Ca for a given sample
scenario A1	scenario for which ΔCa is constant, whilst factors B and AF are adjusted to fit fCa_MgCa to fCa_dCa
scenario A2	scenario for which ΔCa is constant, whilst factors B and AF are adjusted to fit fCa_MgCa to fCa_dCa
scenario A3	scenario for which ΔCa is variable, whilst factors B and AF are adjusted to fit fCa_MgCa to fCa_dCa
scenario "full"	scenario for which AF=1 and B=1, not fit to fCa_δCa
DMg	partitioning coefficient of Mg in calcite
DMg^{o}	partitioning coefficient of Mg in calcite implied by fCa_MgCa with AF=1 and B=1
DMg(fit)	partitioning coefficient of Mg in calcite implied by fCa(fit) as in Eqn. 8

Variable	Description
A	degassing slope from Eqn. 2
$\Delta_{calcite\text{-}dissolved}$, $\Delta^{44}Ca$	Ca isotope fractionation factor ($^{44}Ca/^{40}Ca$)
$\delta^{13}C$ meas	measured stalagmite $\delta^{13}C$ for a given sample
$\delta^{13}C$ init	$\delta^{13}C$ expected in stalagmite prior to degassing and PCP as calculated by Eqn. 2
$\delta^{13}C\_DIC\_init$	$\delta^{13}C$ expected in dripwater prior to degassing and PCP
fCa	modeled fraction of the initial Ca remaining at the time of speleothem carbonate deposition
fCa_δCa	proportion of Ca remaining in solution determined using calcium isotope measurements on the stalagmite
fCa_MgCa	proportion of Ca remaining in solution determined using Mg/Ca measurements on the stalagmite
fCa (fit)	proportion of Ca remaining in solution, calculated from Mg/Ca measurements on the stalagmite with adjustments for compatibility with fCa_δCa
fCa^o	fCa_MgCa with AF=1 and B=1
B	scaling factor to estimate bedrock Mg/Ca from minimum stalagmite measured Mg/Ca, as in Eqn. 6
AF	attenuation factor to transform fCa_MgCa into fCa(fit) as in Eqn. 7
Mg/Ca initial	inferred bedrock Mg/Ca and initial dripwater Mg/Ca
Mg/Ca min	minimum Mg/Ca measured in a given stalagmite
Mg/Ca meas	measured stalagmite Mg/Ca for a given sample
scenario A1, scenario A2	scenario for which ΔCa is constant, whilst factors B and AF are adjusted to fit fCa_MgCa to fCa_dCa
scenario A3	scenario for which ΔCa is variable, whilst factors B and AF are adjusted to fit fCa_MgCa to fCa_dCa
scenario "full"	scenario for which AF=1 and B=1, not fit to fCa_δCa
DMg	partitioning coefficient of Mg in calcite
DMg^o	partitioning coefficient of Mg in calcite implied by fCa_MgCa with AF=1 and B=1
DMg(fit)	partitioning coefficient of Mg in calcite implied by fCa(fit) as in Eqn. 8

2.2 Indicators of PCP

2.2.1 Mg/Ca and Sr/Ca

As discussed previously (Stoll et al., 2012), the signal of PCP imprinted on a stalagmite includes calcite precipitation truly prior to landing ~~impingement~~ of the water drop on the stalagmite surface, as well as the "extent of precipitation" occurring

from the drop on the stalagmite surface before it is displaced from the active growth axis by flow. As the combined signal is manifest in the stalagmite, hereafter we discuss both true PCP and the extent of precipitation processes under the term "PCP". Mg/Ca is the most widely applied indicator of degassing and PCP. Due to the low ~~partitioning~~partition coefficient of Mg in calcite (e.g. as low as 0.012, (Day and Henderson, 2013)), the precipitation of calcite leads to increase in the solution Mg/Ca. The Rayleigh equation (2) relates the fraction of initial Ca remaining in solution (fCa_MgCa) to the initial dripwater Mg/Ca (eg prior to degassing) and measured solution Mg/Ca , when the ~~partitioning~~partition coefficient D is known.

$$(3)\quad f_{Ca\_MgCa} = \frac{Mg/Ca_{speleothem}}{Mg/Ca_{initial} \cdot D_{Mg}}^{\frac{1}{(D_{Mg}-1)}}$$

Figure 2a illustrates an example evolution. Mg/Ca is most robust as a quantitative indicator of PCP in a given stalagmite when the initial dripwater Mg/Ca (prior to degassing) remains constant, and when there is minimal variation in the ~~partitioning~~partition coefficient of Mg. In cave analogue laboratory experiments, ~~the Mg partitioning coefficient~~ D_{Mg} increases by about 17% with a 10°C temperature increase (Day and Henderson, 2013). Additionally, in farmed calcite a 60-70% increase in the D_{Mg} was observed as calcite Mg/Ca increases from 10 to 30 mmol/mol (Wassenburg et al., 2020). If D_{Mg} increases with solution Mg/Ca, it would ~~Such a dependence would serve to~~ amplify the Mg/Ca due to increasing PCP. This dependence of D_{Mg} on Mg/Ca has also been shown in some non-cave analogue laboratory experiments (Alkhatib et al., 2022). For inference of PCP, the measured Mg in the stalagmite should be fully in the calcite and not in detrital minerals, a criteria which can be effectively checked using other detrital sensitive indicators like Al/Ca.

A similar formulation to Eq (1) can be made for other divalent cations with ~~partitioning~~partition coefficients significantly less than 1, such as Sr/Ca and Ba/Ca. The coherence of changes in Mg/Ca, Sr/Ca and to a lesser extent Ba/Ca is often interpreted to signify that PCP is the controlling process(Sinclair, 2011; Wassenburg et al., 2020). Deviations from expected PCP control may reflect variation in the ~~partitioning~~partition coefficients of Sr (or Ba). Increased DSr with higher growth rate or saturation state is widely seen in non-cave analogue laboratory experiments (Tang et al., 2008a; Tesoriero and Pankow, 1996; Lorens, 1981). An up to 5-fold increase in DSr is simulated for a two order of magnitude increase in growth rate (Nielsen et al., 2013) based on ion by ion growth models and non-cave analogue experiments. According to this model, the magnitude of the growth rate dependence depends on the forward and reverse reaction rates, which are sensitive to temperature and solution chemistry. Additionally, in- cave measurements suggest that the DSr increases with increasing calcite Mg/Ca ratio. A tripling of calcite Mg/Ca from 1.4 to 4.2mmol/mol leads to an 18% increase in DSr, and a tripling of Mg/Ca from 10 to 30 mmol/mol leads to an 80% increase in DSr (Wassenburg et al., 2020). A similar increase of DSr with higher Mg/Ca, observed in laboratory growth in a seawater-like matrix, is attributed to the increased accommodation of larger Sr ions in the crystal lattice when the lattice is distorted by incorporation of Mg ions which are smaller than Ca (Mucci and Morse, 1983).

Formatted: Subscript

Formatted: Subscript

Formatted: Subscript

The use of Mg/Ca (or Sr/Ca) as a quantitative indicator of PCP also requires that the initial dripwater Mg/Ca attained by karst rock dissolution prior to PCP remain constant for a given dripwater site and stalagmite over the time period of interest. Yet, in karst rocks composed of heterogeneous carbonate mineralogy, there is potential for variation in initial dripwater trace element/Ca ratios. In karst rocks composed of both dolomite and calcite, the slower dissolution kinetics of dolomite may lead to greater relative dolomite contribution with longer water residence times, leading to higher dripwater Mg/Ca and higher dripwater Mg/Sr with longer water residence times (Tremaine and Froelich, 2013; Fairchild and Treble, 2009). In young reef limestone, primary aragonite and high Mg calcite dissolves more rapidly than diagenetic low Mg calcite, potentially contributing to temporal evolution of initial, undegassed dripwater ratios over time due to progressive meteoric diagenesis of primary phases(Sinclair et al., 2012). Where bedrock is heterogeneous, it can be useful to define the initial (undegassed, without PCP) dripwater chemistry as resulting from the mixture of the multiple bedrock components, e.g. the bedrock mixing fraction (Tremaine and Froelich, 2013). In a synthesis of published dripwater time series, in 30 out of 32 drip locations (from 11 different cave systems), bedrock mixing fractions remained constant to within 3%, and the temporal variations in Mg/Ca were driven by variable extent of PCP(Tremaine and Froelich, 2013). This compilation suggests that in a large majority of investigated settings, for an individual drip, seasonal and interannual variations in water residence time do not significantly affect the initial Mg/Ca attained through karst dissolution. In the cave system from which our example stalagmite records derive, dripwater monitoring similarly suggests stable bedrock mixing fractions at each drip location(Kost et al., 2023).

In monitoring studies, a constant dripwater Mg/Sr ratio over periods of strongly varying drip rate and water residence time, is an indicator of constancy in the proportion of dolomite/calcite dissolution. When partition coefficients of Mg and Sr in speleothems are constant over time, constancy of Mg/Sr ratio of speleothems may be a useful indicator that PCP, rather than differential dissolution, is the main process responsible for Mg/Ca variations(Tremaine and Froelich, 2013). However, variable Mg/Sr in stalagmites may also be caused by strong variations in the partition coefficients of Sr, an interpretation supported by the dependence of stalagmite Mg/Sr and inferred D_{Sr} on growth rate in many stalagmites (Sliwinski et al., 2023). In such cases, variation in stalagmite Mg/Sr ratios does not necessarily indicate variation in the dripwater Mg/Sr ratios or variation in the dolomite/calcite relative contribution. Thus, we suggest that monitoring of dripwater systems may serve as the most meaningful check of the potential stability of the bedrock mixing fraction and initial dripwater trace element/Ca ratios.

Formatted: Space Before: 0 pt

Formatted: Font: Times New Roman, Font color: Auto, English (United Kingdom)

Formatted: Font: Times New Roman, Font color: Auto, English (United Kingdom)

Formatted: Font: Times New Roman, Font color: Auto, English (United Kingdom)

Formatted: Font: Times New Roman, Font color: Auto, English (United Kingdom)

Formatted: Font: Times New Roman, Font color: Auto, English (United Kingdom)

Formatted: Font: Times New Roman, Font color: Auto, English (United Kingdom)

Formatted: Font: Times New Roman, Font color: Auto, English (United Kingdom)

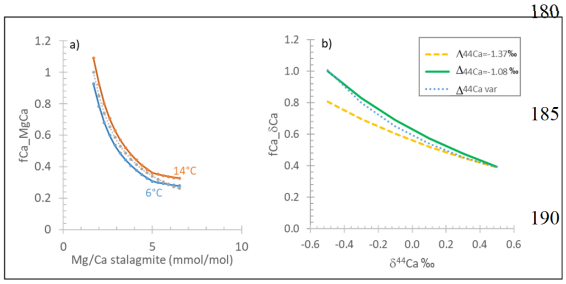

Figure 2. a) . Example variation in Mg/Ca with fCa from Rayleigh simulation of progressive calcite precipitation at 6°C (lowermost curve) and 14°C (uppermost curve) using D_{Mg}~~Mg~~ of (Day and Henderson, 2013); example is shown for Mg/Ca dripwater 400 mmol/mol. Also shown with dashed line is the "index" approximation produced by equation 5. b) Example estimation of fCa from $\delta^{44}Ca$, illustrating effect of fractionation factor on the calculated f_{Ca} for two examples of constant fractionation, and one case in which the fractionation factor systematically evolves from $\Delta_{calcite\text{-}dissolved}$ of -1.37 to -1.08 with increasing PCP and concomitant slowing of growth rate. Example shown for a bedrock $\delta^{44}Ca$ of 0.58.

2.2.2 Calcium isotopes

$\delta^{44}Ca$ has also been employed as an indicator of PCP, since there is a fractionation of Ca isotopes during the dehydration of the ion for it to be incorporated in the crystal lattice. The lighter isotope desolvates more rapidly and thereby is incorporated preferentially in the calcite lattice(Hofmann et al., 2012). Consequently, with progressive removal of Ca into calcite, the remaining dissolved Ca evolves to isotopically heavier composition(Owen et al., 2016) (Figure 2b). The quantitative calculation of fCa from calcium isotopes (fCa_δCa) is most robust when the Ca isotopic composition of the host rock is known and initial $\delta^{44}Ca$ from dissolution is constant (ie always congruent), and when the fractionation factor for Ca isotopes during dehydration and calcite precipitation is constant and known. The fractionation factor may be expressed as α, or as $\Delta_{calcite\text{-}dissolved}$.

Previous applications of $\delta^{44}Ca$ in speleothem studies have focused on the Holocene, and have monitored cave dripwater and farmed calcite to calculate the dissolved-calcite fractionation factor in that particular cave setting and drip site(Owen et al., 2016; De Wet et al., 2021). Studies then apply this constant fractionation factor to calculate fCa_δCa in stalagmite. For fossil, non-active stalagmites, the fractionation factor cannot be measured in farmed calcite and must be assumed or based on information from farmed calcite in the same or similar cave settings. A summary of field and experimental fractionation factors is given in Supplemental~~ry~~ Table 1. In one monitoring study, $\Delta_{calcite\text{-}dissolved}$ of farmed calcite varied among different drips in a modern cave(De Wet et al., 2021). Models of desolvation and attachment during crystal growth suggest that at higher net precipitation rates, the effective fractionation is greater (Depaolo, 2011). This has been observed in non-cave analogue laboratory experiments (Tang et al., 2008b), and simulated in models which suggest that a two order of magnitude increase in net precipitation rates lead to a decrease in $\Delta_{calcite\text{-}dissolved}$ from -0.75 to -1.45 ‰(Mills et al., 2021). According to this model, the magnitude of the growth rate dependence – specifically the absolute range of growth rate at which $\Delta_{calcite\text{-}dissolved}$ varies strongly - depends on the forward and reverse reaction rates which are sensitive to temperature and solution

chemistry(Depaolo, 2011). For a given growth rate, lower temperatures strengthen the water solvation structure, leading to greater fractionation. Laboratory study suggests that a 10 degree cooling leads to a $\Delta_{\text{calcite-dissolved}}$ ~~$_{44\text{-}40\text{Ca}}$~~ decrease of 0.17‰ (Tang et al., 2008b). Yet over a seasonal 7.5C cave air temperature cycle in Heshang Cave, no seasonal difference in $\Delta_{44\text{-}40\text{Ca}}$ was resolved within analytical error (Owen et al., 2016).

2.2.3 Previous comparisons of PCP indicators

Both δ^{44}Ca and Mg/Ca have been simultaneously employed to study Holocene stalagmites (HS4 in Heshang Cave~~), growing about 170 microns/year~~(Owen et al., 2016) (Li et al., 2018) and last interglacial stalagmites from Northern India (Magiera et al., 2019). These studies report ~~In these two settings, there is~~ good quantitative agreement in estimated fCa_δCa and fCa_MgCa. Relative to glacial-interglacial transitions, the Holocene and last interglacial experienced more stable ~~In these settings, in which~~ temperatures, and potentially also more stable ~~and~~ dripwater initial oversaturation, both factors potentially contributing to constant ~~may not have experienced significant variations,~~ calcite-water Δ44Ca fractionation factors ~~may have remained constant~~. ~~Likewise, although Heshang Cave contains dolomite host rock, variations in water/rock contact times did not result in appreciable variation in the initial Mg/Ca from dissolution (ie not significant enough to cause deviation from theoretical expectation).~~ Heshang Cave contains dolomite host rock, and varying water residence times could potentially alter bedrock mixing fraction, altering the initial Mg/Ca of dripwater prior to degassing. However, if this process were significant, it would lead to deviation in the fCa calculated from Mg/Ca compared to that calculated from δ^{44}Ca. The consistency of fCa estimates from Mg/Ca and δ^{44}Ca suggest that variations in water/rock contact times did not result in appreciable variation in the bedrock mixing fraction and initial Mg/Ca from dissolution.

Formatted: Font color: Auto

Formatted: Font: Symbol, Font color: Auto

Formatted: Font color: Auto, Superscript

Formatted: Font color: Auto

Formatted: Font color: Auto

Formatted: Font color: Auto

2.3 Limitations of the Hendy Test for degassing correction

The sampling of calcite precipitated from the same initial dripwater but with progressive degree of CO_2 degassing and calcite removal has often been attempted through extraction of samples in a single growth layer at succesive distances along the growth axis (Hendy, 1971). In theory, the evolution of Mg/Ca and δ^{13}C could be examined along a growth layer. However, in practice it is difficult and often impossible to follow a single growth layer laterally along the stalagmite, especially since growth layer thickness decreases with increasing distance from the main growth axis(Dorale and Liu, 2009). Furthermore, simulations suggest that for a drip interval of 60s, a flow distance in excess of 3 cm from the main axis is required to generate even a 1 permil enrichment of δ^{13}C through PCP and CO_2 degassing (Mühlinghaus et al., 2009). Finally, because the dripwaters experiencing a lot of degassing are less saturated as they flow off axis than drips with little degassing, the off-axis growth may be biased towards times of low degassing and low PCP. For these reasons, it is often impractical to test relationships between δ^{13}C and Mg/Ca using the Hendy test.

3. Methods

3.1 Geochemical models of speleothems

We employ CaveCalc for simulations of equilibrium fractionation of carbon isotopes. The CaveCalc package employs the PHREEQC geochemical model to simulate the initial dissolution of karst limestone in equilibrium with a given volume of soil gas of specified pCO_2 and $\delta^{13}C$, and the subsequent equilibration of this solution with a cave atmosphere of specified pCO_2 leading to precipitation of $CaCO_3$. Relevant for this study, the CaveCalc package calculates the initial $\delta^{13}C$ of bicarbonate and initial Ca concentration of the dripwater resulting from karst dissolution, and the stepwise evolution of both parameters as well as the $\delta^{13}C$ of the precipitated calcite as the solution equilibrates with the cave atmosphere. These CaveCalc simulations allow us to relate the Rayleigh-driven progressive enrichment in $\delta^{13}C$ of bicarbonate with the progressive depletion of Ca in the dripwater in equilibrium conditions. CaveCalc employs the temperature dependent calcite- HCO_3^- fractionation as calculated by (Mook and Rozanski, 2000).

Independent from CaveCalc, a modified version of the I-STAL model (Stoll et al., 2012) is used to simulate PCP variation resulting from changes in initial dripwater saturation state, and changes in drip interval. The effect of variations in initial dripwater Ca, temperature, and drip interval are explored at conditions of cave pCO_2 fixed at ventilated, near interglacial atmospheric concentrations (300 ppm). In I-STAL calculations, the temperature sensitivity of D_{Mg}~~Mg~~ follows (Day and Henderson, 2013).

3.2 Analysis of fossil stalagmites

We compile existing and report new data on 9 stalagmites from NW Spain with growth periods during the Holocene, during late MIS 5, and during the penultimate deglaciation (Supplemental Tables 2 and ~~2~~3). Reported stalagmites are from La Vallina Cave, whose setting and lithology are described in a detailed previous monitoring study(Kost et al., 2023) ~~(Kost et al)~~. The cave is hosted in Carboniferous limestones of the Barcaliente Formation. Because the section is dipping at 80°, different sectors of the cave sample stratigraphically different portions of the limestone, which have significant heterogeneity in Mg/Ca and some heterogeneity in Sr/Ca and other trace elements. Thus, different drip locations can feature different initial trace element ratios due to congruent dissolution of limestones of differing composition. Despite site to site heterogeneity, individual drips monitored over an 18 month period show very limited temporal variation in Mg/Sr ratios despite order of magnitude differences in drip rate, suggesting that in this cave, individual drips sample a relatively stable bedrock dissolution source and maintain a constant bedrock mixing fraction. For most stalagmites, age models are published previously, including those for GAE, GAL, and GLO (Stoll et al., 2015; Stoll et al., 2013), GAR and GUL (Stoll et al., 2022). For BEL, GLD, and ROW, age model constraints are given in the Supplemental~~ry~~ Table 2. The slowly growing fossil stalagmites consist of dense calcite and show no evidence for columnar porous fabrics. Stalagmite calcite for GAR and GAL consist of predominantly columnar compact to columnar open fabrics (Sliwinski and Stoll, 2021). Similar fabrics are confirmed in GUL and GAE(Sliwinski et al., 2023). Samples ROW, BEL, and NYM fall exhibit growth rates (12-40 µm/yr) similar to GAR, GAL,

Formatted: Font: Times New Roman, Font color: Auto

Formatted: Font: Times New Roman, Font color: Auto, English (United Kingdom)

Formatted: Font: Times New Roman, Font color: Auto

Formatted: Font: Times New Roman, Font color: Auto, English (United Kingdom)

Formatted: Font: Times New Roman, Font color: Auto, English (United Kingdom)

Formatted: Font: Times New Roman, Font color: Auto, English (United Kingdom)

Formatted: Font: Times New Roman, Font color: Auto, English (United Kingdom)

Formatted: Font: Symbol

Formatted: Font: Times New Roman, Font color: Auto, English (United Kingdom)

Formatted: Font: Times New Roman, Font color: Auto, English (United Kingdom)

GUL, and GAE and feature similar dense, nonporous macroscopic textures. The much more slowly growing GLO and GLD likewise feature dense, compact calcite comparable to sample GLA with similar growth rate and described as columnar and columnar open(Kost et al., in review)~~(Kost et al., 2023)(Kost et al., in review)~~.

For geochemical analyses, we sampled approximately 1 mg of powder. Trace element ratios (Mg/Ca, Sr/Ca) were determined by dissolution of powders in 2% HNO3 and analysis on Agilent 8800 ICP-MS at ETH Zurich in collision mode. On splits of the same powders, we measured $\delta^{13}C$ and $\delta^{18}O$ using a Thermo Fisher Scientific Gas Bench II with methods previously described and precision of 0.08‰for both isotopes (Breitenbach and Bernasconi, 2011).

In 8 stalagmites, we selected several intervals of con~~s~~trasting Mg/Ca to additionally measure $\delta^{44}Ca$. From the same aliquot used for Mg/Ca analysis, ~500 µg of powder was dissolved in distilled 2M HNO_3. An automated Ca-Sr separation method (PrepFAST MC, Elemental Scientific, Omaha, NE, USA) was used to separate Ca from Sr, Mg and other matrix elements, to avoid isobaric interferences during multi-collector inductively coupled mass spectrometry (MC-ICP-MS). SRM 915b solutions were purified in parallel with the samples to provide a combined column-chemistry and analytical accuracy assessment. Ca-isotope ratios were determined using a Nu Instruments MC-ICP-MS (the University of Oxford) with a desolvating nebulizer as described previously~~.~~ (Reynard et al., 2011). ~~-~~Solutions were run at 10 ± 1 ppm concentration, and the sample~~sample~~s were measured with standard-sample bracketing. A minimum of 5 analyses were conducted on each aliquot~~sample~~. δ44/40Ca is reported normalized to NIST SRM 915a and was calculated from measured $\delta^{44/42}Ca$, as $\delta^{44/40}Ca = \delta^{44/42}Ca * ((43.956-39.963)/(43.956-41.959))$(Hippler et al., 2003). To determine accuracy and external precision, secondary standards NIST SRM 915b and HPSnew (in-house standard) were used. Uncertainty on Ca isotope data is quoted as the t-distribution-derived 95% confidence interval on the mean of repeat measurements calculated using either the standard deviation on all repeat measurements on each sample.

Additionally, we incorporate published $\delta^{13}C$, fCa_δCa, and Mg/Ca data from Heshang stalagmite HS4(Owen et al., 2016; Noronha et al., 2014).

3.4 Calculation of fCa from $\delta^{44}Ca$, Mg/Ca and Sr/Ca

Mg/Ca measurement is much faster than $\delta^{44}Ca$, and therefore it is common to have Mg/Ca measured for every $\delta^{13}C_{init}$ measured in the stalagmite We therefore carry out examples employing Mg/Ca as~~is~~ the preferred measurement for deriving a continuous record of $\delta^{13}C_{init}$ ~~because measurement is much faster and therefore it is common to have Mg/Ca measured for every $\delta^{13}C_{init}$ measured in the stalagmite~~. At the same time, using $\delta^{44}Ca$ to derive the PCP-corrected $\delta^{13}C_{init}$ may be more robust, because the $\delta^{44}Ca$ of the initial solution can be derived from the measured bedrock and the isotopic composition of the bedrock is expected to be more homogeneous than Mg/Ca leading to less uncertainty in the initial solution, and because Ca is a major element.

We calculate fCa_δCa from $\delta^{44}Ca$ measurements using a constant bedrock $\delta^{44}Ca$ equal to average bedrock (0.58‰) reported previously (Lechleitner et al., 2021b). Use of the highest or lowest measured bedrock $\delta^{44}Ca$ leads to a +/- 0.05 range in

Formatted: Font: Times New Roman, Font color: Auto, English (United Kingdom)

Formatted: Font: Times New Roman, Font color: Auto, English (United Kingdom)

Formatted: English (United States)

absolute fCa_δCa values. Because bedrock $\delta^{44}Ca$ is not expected to change at a given location over time, we do not expect this factor to contribute to temporal variations in $\delta^{44}Ca$. The $\Delta_{calcite\text{-}dissolved}$. for these fossil stalagmites is not independently constrained. Therefore, we complete a sensitivity analysis using the range of $\Delta_{calcite\text{-}dissolved}$. observed in laboratory calcite growth and ion by ion growth models. Supplemental~~ry~~ Table 1 lists the 4 values of $\Delta_{calcite\text{-}dissolved}$. which we evaluate.

Inference of the fCa_MgCa from Mg/Ca using the Rayleigh formula requires knowledge of the ~~partitioning~~partition coefficient and the initial dripwater Mg/Ca, which are both difficult to infer for fossil stalagmites.

Because the D_{Mg}~~Mg~~ is very low, and the exponent in the Rayleigh formula (Equation 3) is therefore very close to -1, the following provides a close approximation for fCa: :

(4) $$f_{Ca\_MgCa} = \frac{MgCa_{initial}}{MgCa_{sample}}$$

For a D_{Mg}~~Mg~~ of 0.025, this approximation deviates from the Rayleigh equation by 0.01 at fCa =0.36 and deviates by lesser degrees for higher fCa_MgCa (e.g. gray dashed line in Figure 2a).

Because of heterogeneity in cave bedrock, we calculate fCa_MgCa assuming there may be differences in the initial dripwater Mg/Ca for each stalagmite location. Time series data for each stalagmite indicates a range of Mg/Ca values. In a first approach, we assume that the minimum Mg/Ca of a stalagmite corresponds to a situation of negligible degassing and PCP, and that the D_{Mg}~~Mg~~ is constant, and therefore that the numerator can be approximated by the minimum Mg/Ca for the stalagmite:

(5) $$f_{Ca\_MgCa} = \frac{MgCa_{min}}{MgCa_{sample}}$$

By default in this approximation, the maximum fCa_MgCa calculate for any stalagmite is 1. Therefore, we consider the consequences for calculated fCa_MgCa if the measured minimum Mg/Ca in the stalagmite corresponds to precipitation from a solution which has already experienced PCP. We assess this impact with a scaling factor B (between 0.5 and 1) to approximate the initial bedrock dissolution Mg/Ca from the minimum Mg/Ca measured in the stalagmite, and apply a constant B for the stalagmite:

(6) $$MgCa_{initial} = MgCa_{min} * B$$

fCa_SrCa may also be calculated from Sr/Ca measurements in an approach analogous to Mg/Ca. Because of the higher DSr, Equation 5 is a less accurate approximation for Sr, eg for a DSr of 0.1, there would be a 0.04 deviation of the fCa_SrCa by Eq. 5 (fCa =0.30) compared to the Rayleigh formula at fCa_SrCa=0.265

Finally, we also evaluate the possibility of temporal variation in D_{Mg}~~Mg~~ in a given stalagmite, testing the scale of variation in D_{Mg}~~Mg~~ which would be consistent with fCa_δCa estimations from $\delta^{44}Ca$. In this fCa(fit), the curvature or slope of the relationship in Figure 2a is modified by an attenuation factor AF.

(7) $$f_{Ca\,(fit)} = B - \left(\frac{\left(B - \frac{MgCa_{initial}}{MgCa_{sample}} \right)}{AF} \right)$$

The relative change in D_{Mg}~~Mg~~ needed for the fit is given as:

$$\frac{D_{Mg(fit)}}{D_{Mg^\circ}} = \frac{f_{Ca(fit)} MgCa_{init^\circ}}{f_{Ca^\circ} MgCa_{init(fit)}} \quad (8)$$

Where fCa° indicates the fCa_MgCa for the full scenario, with AF=1 and B=1. This AF gives a linear increase in D_{Mg}~~DMg~~ with Mg/Ca, however other forms of dependence could also fit the data, since we have $\delta^{44}Ca$ for only 2 points for most of the analyzed stalagmites.

3.5 Estimation of $\delta^{13}C_{init}$ from $\delta^{13}C_{meas}$ and estimated fCa

We use Mg/Ca to derive continuous PCP-corrected $\delta^{13}C_{init,}$ but we employ the few existing $\delta^{44}Ca$ measurements for each stalagmite to validate and adjust the precise relationship between Mg/Ca and PCP yielding fCa (fit) in order to achieve a more robust estimate of $\delta^{13}C_{init.}$ In detail, we use the Mg/Ca to calculate fCa in 4 different ways: fCa_MgCa from the minimum stalagmite Mg/Ca and constant D_{Mg}~~DMg~~ (termed "full" with both B and AF=1), and additionally from three other fCa(fit) using equation 7 (termed "A1, A2, and A3") in which the parameters B and AF are adjusted to provide fCa_MgCa compatible with fCa_δCa. For each stalagmite, the values of B and AF employed for A1, A2, and A3 are given in Table 2~~3~~.

For each of these four possible fCa scenarios, we additionally calculate $\delta^{13}C_{init}$ using three possible values of the degassing slope (A) in equation 3: -5, -8, and -11 ‰ (e.g. in Figure 2b). This exercise illustrates the consequences of a range of possible equilibrium and disequilibrium fractionation behaviors.

4. Results

4.1 PCP indicators in stalagmites

Within the subsamples measured for both Mg/Ca and $\delta^{44}Ca$, the $\delta^{44}Ca$ of measured samples ranges from -0.49 to +0.42. In all of these subsets, the Mg/Ca and $\delta^{44}Ca$ positively correlate (Figure 3). In all but two stalagmites, Sr/Ca and $\delta^{44}Ca$ positively correlate. In GUL and GAL, Sr/Ca and $\delta^{44}Ca$ negatively correlate.

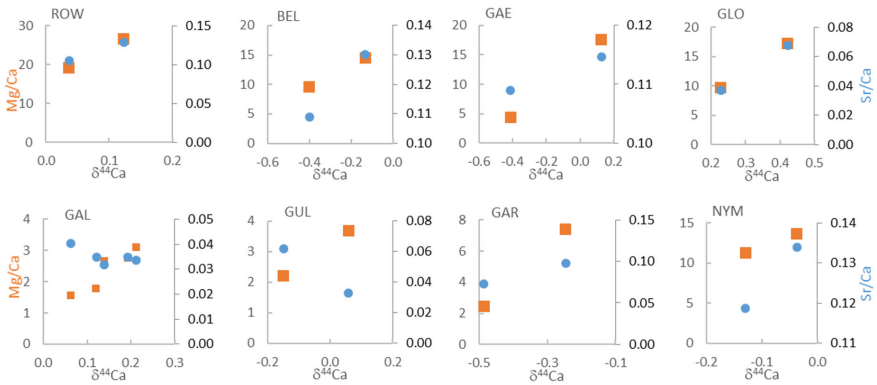

Figure 3. Mg/Ca (orange squares on left axes, in mmol/mol) and Sr/Ca (blue circles on right axes, mmol/mol) vs δ^{44}Ca (‰) for paired samples from each stalagmite.

In the ~~Across the~~ full geochemical sampling of the 9 examined~~8~~ speleothems from La Vallina~~Porrua~~ Cave, ~~the total range in~~ Mg/Ca variation in a given stalagmite ranges between ~~across each speleothem is between~~ 1.7-fold and 3.5-fold, with the exception of ~~in all speleothems except~~ GAE (12.2-fold range) Six of the 9 stalagmites ~~; 5 of the stalagmites~~have Mg/Ca variations of 2-fold to 3-fold ~~have a range between 2 and 3~~ (Supplemental Table 3~~2~~). The 1.7 to 3.5 fold range could be fully explained by PCP even with no change in D_{Mg}~~DMg~~, since a 3.5 fold range requires the initial dripwater Ca concentration to be greater than 3.5 times the saturation Ca concentration for the cave conditions. Changes in the Mg/Ca of the initial dripwater, prior to degassing, from varying bedrock mixing fraction~~process such as enhanced water rock interaction~~, or enhanced Mg/Ca ratio due to increased fluid inclusion density, are not required to attain the range of Mg/Ca in 7 of the 8 of the stalagmites. With the exception of Holocene GAL, minimum Mg/Ca generally occurs during the glacials and stadials (Supplemental Table 3~~2~~). In GAE, the basal 0.5 cm of the stalagmite feature an unusually low Mg/Ca ratio which is 12-fold lower than the maximum ratio. If driven solely by PCP, this range would require dripwater Ca in excess of 300 ppm during warm periods to drive such a large range in PCP. In this stalagmite, the Mg/Ca of this basal portion may reflect a different initial state of the fracture network and mineral surface age over time. GAE was sampled growing on a large block fallen from the ceiling and first growth after block emplacement may reflect flow through newly opened fracture networks.

The total range in Sr/Ca across each speleothem is between 1.7-fold ~~–~~and 4-fold in all speleothems except GAE (6) (Supplemental Table 3~~2~~). The strongest positive correlation between Sr/Ca and Mg/Ca is found in GLO, GLD, and BEL. Strong negative correlation occurs in GUL, and modest negative correlation occurs in GAL and GAR.

~~**Table 2: Sample information and trace element summary.**~~

stalagmite	period included in this study	age base and tip	min Mg/Ca (mmol/mol)*	age min Mg/Ca (ka)	max Mg/Ca (mmol/mol)	age max Mg/Ca (ka)	range Mg/Ca (max/min)	min Sr/Ca (mmol/mol)	max Sr/Ca (mmol/mol)	range Sr/Ca (max/min)	Correlation Sr/Ca and Mg/Ca**
GAL	9-4 ka, 26 ka	26 ka, 1 ka	1.1	2	3.8	6	3.5	0.023	0.054	2.3	-0.29
GUL	14.5 - 4 ka	14.5 ka to 4 ka	1.6	14	4.1	5	2.5	0.026	0.065	2.5	-0.71
GAE	94-82 ka	135 ka to 73 ka	2.2	143	26.3	129, 97	12.2	0.025	0.162	6.5	0.37
GAR	140-125ka	217 ka to 112 ka	2.8	145	8.5	127	3.0	0.028	0.094	3.3	-0.34
GLO	94-82 ka	196 ka to 84 ka	7.6	166	22.5	85	3.0	0.020	0.081	4.0	0.68
BEL	140-125ka	172 ka to 128 ka	9.1	134	25.3	131	2.8	0.076	0.247	3.3	0.72
NYM	MIS 5e	148 ka to 113 ka	9.3	115	18.6	122	2.0	0.088	0.162	1.8	0.45
ROW	94-82 ka	107 ka to 82 ka	18.1	108	30.4	81	1.7	0.095	0.156	1.6	-0.1
GLD	140-125ka	141 ka to 99 ka	18.8	136	40.0	96	2.1	0.066	0.153	2.3	0.77
*including all analyses for the given stalagmite											
** over the period of interest											

4.4 Calculated fCa from PCP indicators

4.4.1. Expected ranges in fCa

Because highly oversaturated dripwaters have a greater potential for PCP than minimally oversaturated dripwaters, fCa can vary over a wider range in settings with high oversaturation (e.g. warm climates with higher soil CO_2 and initial dripwater Ca; Figure 4a). In contrast, minimum degassing and high fCa will be favored by very low oversaturation state of the drip, even for slow drip rates (Figure 4a, b). Minimal degassing is also favored by colder temperatures. In the mid and high latitudes, low oversaturation of dripwaters and low PCP are more likely during cold glacial or stadial time periods when CO_2 in soils is depressed due to low temperatures (e.g Fig. 4b). We consider this expected association of colder climates and higher fCa in the quantitative interpretation of fCa indices. Alternatively, when soil pCO_2 and dripwater initial saturation are regulated by the moisture limitation of soils, then fCa varies over a narrower range at constant drip interval (Fig. 3b). We simulate fCa as low as 0.15 in the case of an initial Ca concentration of 137 ppm.

In addition to the oversaturation state, PCP is also dependent on the degassing time. PCP can occur in air-filled voids above the cave as well as on walls and ceilings of the cave prior to the landing of dripwater on the studied stalagmite. Here, we discuss the integrated PCP, regardless of where along the flow path PCP has occurred. The susceptibility of a given speleothem to PCP may depend on the geometry of the flow path. Temporal variations in PCP in a given stalagmite are expected to depend on the flow (e.g. drip rate) as well as on the oversaturation. Because the relationship between drip interval and PCP is known to be highly nonlinear (Fig 4c, d), different coeval stalagmites often have asynchronous variations in PCP indicators or contrasting magnitudes of PCP variation.

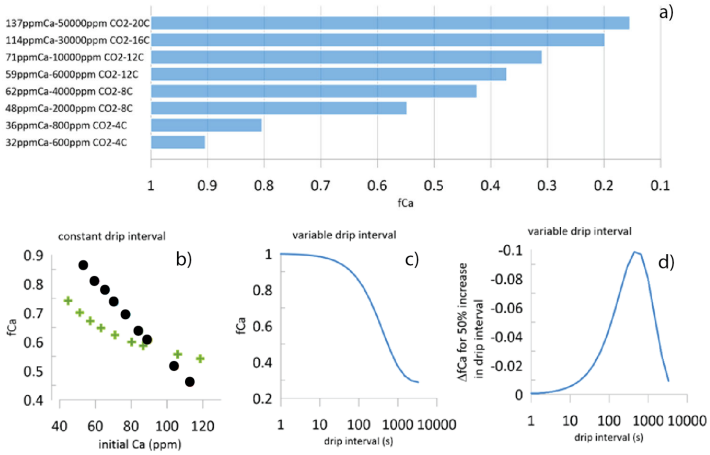

Figure 4. a) The degree of PCP which is possible based on the initial dripwater saturation state simulated by CaveCalc for the initial ppm Ca, soil pCO2 for 150 L gas volume, and reaction temperature. The lowest fCa is defined as that which would correspond to an instantaneous calcite deposition rate equivalent to 4 µm/year, as simulated in I-STAL with Dreybrodt(Romanov et al., 2008) kinetics. b) the fCa simulated for a fixed drip interval of 300 s, but variable initial saturation (indexed by Ca concentration). In one case shown with circles, the variable initial Ca corresponds with a progressive decline in temperature from 18°C to 5°C simulating soil pCO_2 limited by temperature. In a second case shown with green crosses, variable initial Ca corresponds to constant temperature, simulating soil pCO_2 limited by moisture at constant temperature. Simulations assume Dreybrodt kinetics (Romanov et al., 2008)executed in I-STAL with PCP enhancement factor of 3. c, d) Illustration of nonlinearity of PCP relative to drip interval, simulated with Dreybrodt kinetics at temperature 12C, initial Ca 90 ppm, d=0.01 and PCP enhancement factor of 3. The drip interval range of maximum PCP sensitivity will vary with modeled temperature and PCP enhancement parameters.

4.4.1 $\delta^{44}Ca$

The absolute fCa_δCa calculated from a given $\delta^{44}Ca$ depends on the choice of calcite-dissolved fractionation factor (Supplemental Table 1). Given bedrock estimated at 0.58 ‰, the measured $\delta^{44}Ca$ in some samples would imply an fCa_δCa higher than one for the $\Delta^{44}Ca$ fractionation factor corresponding to slowest laboratory growth rates (-0.66.). For a given stalagmite, choice of a $\Delta^{44}Ca$ corresponding to slower laboratory growth rates (-0.66, -0.86) yields a wider range of calculated fCa_δCa than choice of $\Delta^{44}Ca$ corresponding to faster laboratory growth rates (-1.08, -1.37). The largest range in fCa_δCa is found in GAE, and for a given $\Delta^{44}Ca$, the lowest average fCa_δCa are in GAL and GLO (Figure 5, Appendix A). Because the fractionation factor depends on growth rate and the solution characteristics, it may not be constant throughout the growth period of a stalagmite if there are significant changes in the growth conditions. For a given stalagmite, slower growth rate during periods of low initial dripwater oversaturation might be characterized by less fractionation e.g. a Δ44Ca which is closer to 0, compared to periods of stalagmite growth from solutions with greater oversaturation.

Formatted: Superscript
Formatted: Superscript
Formatted: Superscript
Formatted: Superscript

4.4.2 Mg/Ca and Sr/Ca

Using Equation 4 and the minimum Mg/Ca for each stalagmite as an estimation of a nondegassed, fCa_MgCa=1, the high Mg/Ca stalagmites BEL and ROW exhibit a range in fCa_MgCa from 0.95 to 0.6 (Figure 5; Appendix A) and GLO exhibits a similar range (Appendix A). As commented previously, in GAE, the total Mg/Ca range exceeds that expected from PCP if the minimum Mg/Ca in the basal growth phase is used. We complete sensitivity analysis calculating fCa_MgCa of GAE with the 5th percentile value rather than minimum, which is equivalent to the minimum Mg/Ca observed in the upper 82 cm of the stalagmite, including the period of interest presented here. Garth exhibits the highest range in fCa_MgCa estimated from measured Mg/Ca. A smaller range of fCa_MgCa and lowest fCa_MgCa is calculated from Equation 6 when the B factor is <1.

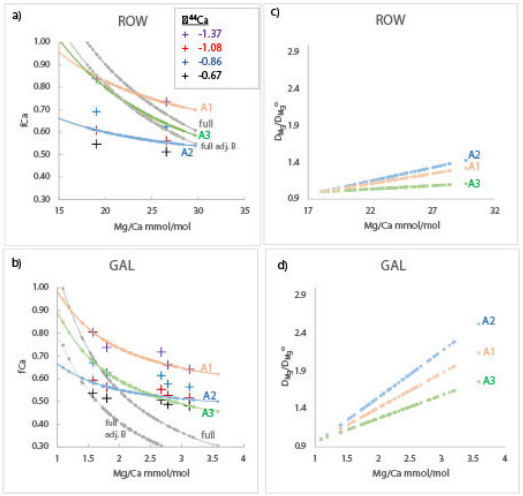

Figure 5. a)-b) fCa_δCa (crosses) and fCa_MgCa and fCa(fit) (both with lines) vs measured Mg/Ca. Crosses show fCa_δCa calculated from $\delta^{44}Ca$ according to different $\Delta^{44}Ca$ fractionation factor, vertically ordered according to fractionation factor as given in the legend. Gray curves show calculation of fCa_MgCa from Mg/Ca assuming Mg/Ca_{min} reflects undegassed dripwater ("full", upper gray line) or that undegassed dripwater is lower than minimum Mg/Ca by factor from 0.65 to 0.95 ("full adj. b", lower gray line; value in ~~Supplemental~~ Table 2~~1~~). Pink, blue,and green lines illustrate scenarios A1, A2, and A3 which are potential relationships between fCa(fit) and Mg/Ca consistent with fCa_δCa estimates according to Equation 7 and fit parameters in Table 2~~3~~. c)-d) The variation in D_{Mg}~~DMg~~ implied by scenarios in a)-b),calculated as in Equation 8 and assuming constant congruent bedrock dissolution to yield a constant initial undegassed Mg/Ca ratio of dripwater. A 10°C temperature increase would cause D/D_o to reach 1.22 according to laboratory experiments(Day and Henderson, 2013).

4.4.3 Comparison of fCa estimations

We explored which combinations of $\Delta^{44}Ca$ and assumptions of B and AF lead to coherent estimations of fCa_δCa and fCa_MgCa of yield fCa(fit). We find that in many stalagmites, with AF=1 the Mg/Ca leads to a wider range in fCa_MgCa than fCa_δCa (e.g. Figure 5, supplemental Figure 1). Covariation in D_{Mg}~~DMg~~ with Mg/Ca is one process which could cause AF to be greater than 1.

Estimates of fCa_δCa and fCa_MgCa for stalagmites BEL, ROW, and NYM are consistent with no systematic variation in D_{Mg}~~DMg~~ (ie an AF ≈1) if the calcite-dissolved fractionation factor $\Delta^{44}Ca$ varies by 0.2‰ between the sample of lowest and

Formatted: Superscript

Formatted: Superscript

highest PCP (Scenario A3; Figure 5, Table 23). Alternatively, if the $\Delta^{44}Ca$ were constant (Scenario A1, A2), then fCa_δCa and fCa_MgCa estimates are consistent only when AF is 1.25 to 3, which imply a systematic variation in D_{Mg}~~DMg~~ with Mg/Ca (Figure 5). For other stalagmites (Supplemental Figure 1), if the calcite-dissolved fractionation factor $\Delta^{44}Ca$ varies by 0.2‰ between the sample of lowest and highest PCP (Fit A3), some variation in D_{Mg}~~DMg~~ is still required (AF 1.5-2.2); for assumption of constant $\Delta^{44}Ca$ in each stalagmite, a larger range of AF is required (1.5 to 3, with a single higher value of 4 required for GAR). For GAE, only choice of a Mg/Camin of 6 mmol/mol, the 5th percentile value, enabled calculation of PCP factor consistent with $\delta^{44}Ca$.

The concomitant changes in D_{Mg}~~DMg~~ for these scenarios ranges from 1 (eg constant D_{Mg}~~DMg~~) to over 2.5-fold increase in D_{Mg}~~DMg~~ over the range of Mg/Ca in the stalagmite (Figure 5). GAL and GAR have the most significant increases in D_{Mg}~~DMg~~, wherease BEL, NYM, and ROW feature the lowest. Most scenarios require an increase in D_{Mg}~~DMg~~ larger than that expected from reasonable (5 to 10 degree) temperature dependence of D_{Mg}~~DMg~~ alone; for example according to experimental cave-analogue calculation, a 10 degree warming would lead to a $D_{Mg}/D_{Mg}o$ of 1.22(Day and Henderson, 2013). Holocene stalagmite GAL features large simulated range in D_{Mg}~~DMg~~ despite only limited regional temperature change.

We acknowledge that we have limited fCa_δCa for each stalagmite, and therefore our particular scenarios are intended to illustrate potential compatible solutions but do not cover all the possible ranges. The variation in D_{Mg}~~DMg~~ may be exaggerated because datasets with higher numbers of paired $\delta^{44}Ca$ and Mg/Ca such as GAL show coherency but also some scatter around this relationship, which may be interpreted as a steeper or shallower relationship in our limited dataset.

Table ~~3.~~2 Parameters for elaboration of fCa based on $\delta^{44}Ca$ and Mg/Ca

			Scenarios									
	full	B1	A1			A2			A3			
	B	B	Δ44Ca	B	AF	Δ44Ca	B	AF	Δ44Ca (1)	D44Ca (2)	B	AF
GAL	1	0.75	-0.66	0.95	2	-1.08	0.65	3	-0.66	-0.86	0.85	1.5
GUL	1	0.75	-1.08	0.95	2	-1.37	0.75	2	-1.08	-1.37	0.95	1.7
GLO	1	0.8	-0.66	0.75	1.5	-1.08	0.57	2	-0.66	-0.86	0.65	1.5
GAR	1	0.85	-1.08	1	3	-1.37	0.8	4	-1.08	-1.37	0.95	2.2
ROW	1	0.9	-0.66	0.87	2	-1.08	0.62	3	-0.66	-0.86	0.87	1.2
NYM	1	0.85	-0.86	1	1.25	-1.08	0.65	3	-0.86	-1.08	1	1
BEL	1	0.8	-1.08	0.95	1.5	-1.37	0.65	3	-1.08	-1.37	0.95	1
GAEL*	1	0.75	-1.08	1	1.5	-1.37	0.9	1.5	-1.08	-1.37	1	1.3
GLD				0.95	1.5		0.95	1			0.65	3
HES				1	1.2		0.9	1.1			0.95	1

*fit with Mg/Camin substituted by Mg/Ca 5th percentile value of 6 mmol

Formatted: Superscript

Formatted: Superscript

Formatted: Superscript

	Scenarios											
	full	B1	A1			A2			A3			
	B	B	$\Delta^{44}Ca$	B	AF	$\Delta^{44}Ca$	B	AF	$\Delta^{44}Ca$ (1)	$\Delta^{44}Ca$ (2)	B	AF
GAL	1	0.75	-0.66	0.95	2	-1.08	0.65	3	-0.66	-0.86	0.85	1.5
GUL	1	0.75	-1.08	0.95	2	-1.37	0.75	2	-1.08	-1.37	0.95	1.7
GLO	1	0.8	-0.66	0.75	1.5	-1.08	0.57	2	-0.66	-0.86	0.65	1.5
GAR	1	0.85	-1.08	1	3	-1.37	0.8	4	-1.08	-1.37	0.95	2.2
ROW	1	0.9	-0.66	0.87	2	-1.08	0.62	3	-0.66	-0.86	0.87	1.2
NYM	1	0.85	-0.86	1	1.25	-1.08	0.65	3	-0.86	-1.08	1	1
BEL	1	0.8	-1.08	0.95	1.5	-1.37	0.65	3	-1.08	-1.37	0.95	1
GAEL*	1	0.75	-1.08	1	1.5	-1.37	0.9	1.5	-1.08	-1.37	1	1.3
GLD				0.95	1.5		0.95	1			0.65	3
HES				1	1.2		0.9	1.1			0.95	1

*fit with Mg/Camin substituted by Mg/Ca 5th percentile value of 6 mmol

4.5 Estimation of $\delta^{13}C_{init}$ in measured speleothems

Following the use of Scenarios A1, A2, and A3 to generate the fCa used in Equation 3, we generated time series records of $\delta^{13}C_{init}$ for 8 stalagmites spanning three time periods of interest - the Late glacial to Holocene, the penultimate glacial to interglacial transition, and a stadial event occurring between 87 and 85 ka BP. For clarity in time series figures, we illustrate the three scenarios only for the -8‰ degassing slope. For one scenario (A1) we illustrate the range in $\delta^{13}C_{init}$ for degassing slopes from -5 to -11‰. This range is variable over time in a given stalagmite, because the choice of degassing slope (-5, -8, -11‰) impacts the $\delta^{13}C_{init}$ significantly for low fCa and to a lesser degree for higher fCa.

We begin by comparing the range of $\delta^{13}C_{init}$ calculated for growth during interglacials, and the present the time series trends for select individual stalagmites ~~(time series for the remaining stalagmites are illustrated in the supplement)~~.

4.5.1 Interglacials

The median $\delta^{13}C_{init}$ among interglacial samples (here averaging 9-4 ka; and 129 to 125 ka) is strongly dependent on the degassing fractionation slope A (Figure 6). For the three fCa scenarios (A1, A2, A3) in which Mg/Ca-based fCa is attenuated for consistency with $\delta^{44}Ca$, with a -5‰ slope, median $\delta^{13}C_{init}$ ranges from -9 to -13‰ and for the -11‰ slope, $\delta^{13}C_{init}$ is in the -11.5 to -16‰ range. For scenario full, the -5 ‰ and -8 ‰ $\delta^{13}C_{init}$ overlap with modern nondegassed calcite predicted from $\delta^{13}C_{DIC}$ measurements, whereas for -11 ‰, scenarios A1 and full lead to $\delta^{13}C_{init}$ which is 5 to 7 ‰ more negative than modern $\delta^{13}C$ calcite of undegassed drip. Use of the "full" fCa scenario with no attenuation of the fCa from Mg/Ca and the slope of -11 ‰ leads to extreme negative $\delta^{13}C_{init}$ for GAR, GAL, GUL, and GAE but not BEL or GLD. With this fCa scenario, slopes -5 or -8 ‰ yield $\delta^{13}C_{init}$ within the ranges described above.

4.5.2 Three coeval time series during MIS 5 b-c

Three stalagmites spanning 94 to 82 ka interval feature contrasting trends in measured $\delta^{13}C$ (Figure 7). An excursion to more positive measured $\delta^{13}C$ is noted around 89 to 86 ka BP in GLO, the stalagmite with the most constant Mg/Ca. However, the brief positive anomaly is not well expressed in measured $\delta^{13}C$ GAE because of a high amplitude long term trend over this time interval. Yet, in $\delta^{13}C_{init}$, all three stalagmites show a similar positive anomaly. The $\delta^{13}C_{init}$ with slopes -8 or -11, for all fCa scenarios, leads to a double structure positive $\delta^{13}C$ anomaly at 89 to 86 ka, and a constant background $\delta^{13}C$init from 94 to 82 ka. The $\delta^{13}C_{init}$ for these simulations in GAE exhibits a more similar trend to that of GLO and ROW.

A comparison of the range of fCa in each scenario, the resulting range in $\delta^{13}C_{init}$, and the correlation of measured $\delta^{13}C$ with the $\delta^{13}C_{init}$ is given in Supplemental Figure 2~~illustrated in Figure 7 panels f, g, and h~~. The most pronounced change between measured $\delta^{13}C$ and the $\delta^{13}C_{init}$ is simulated for GAE, in which correlation of $\delta^{13}C_{init}$ and measured $\delta^{13}C$ is below 0.2 for all degassing slopes except -5‰. The case of GAE contrasts with that of GLO, in which the correlation remains above 0.5 for all scenarios consistent with $\delta^{44}Ca$ (eg scenarios A1, A2, and A3). This reflects the greater range in fCa for GAE than for GLO.

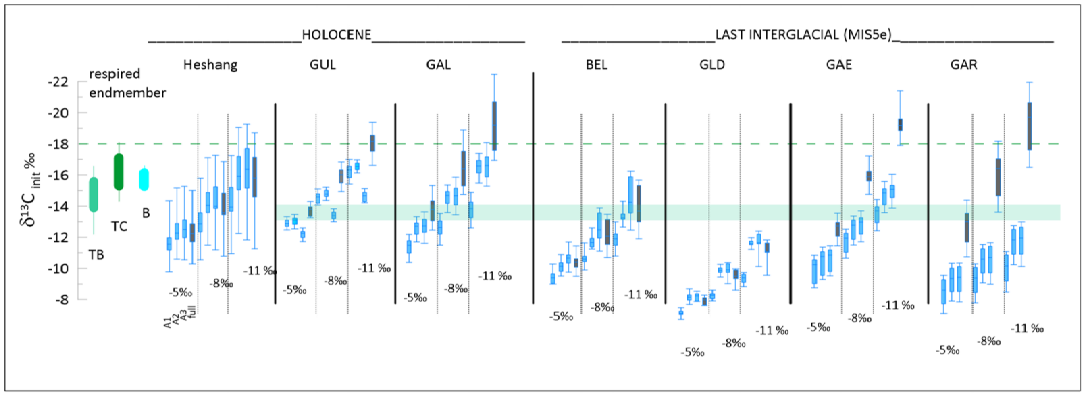

Figure 6. Comparison of calculated $\delta^{13}C_{init}$ for interglacial samples spanning 9 to 5 ka and 129 to 125 ka with the calculated composition for calcite for modern $\delta^{13}C_{DIC}$ composition under forested portions of the cave (green horizontal band), as well as the calcite calculated for limited degassing of dripwaters equilibrated with soil pCO_2 (10000ppm) of composition consistent with the $\delta^{13}C$ of respired endmembers in temperate broadleaf (TB), temperate conifer (TC) and boreal (B) ecosystems (Pataki et al., 2003) illustrated as vertical ranges . For each stalagmite, the whisker plots show distribution of $\delta^{13}C_{init}$ for three fCa scenarios consistent between Mg/Ca and $\delta^{44}Ca$ (A1, A2, A3; blue shading) as well as the fCa derived from the full, unadjusted Mg/Ca record (gray shading) for three different degassing slopes. Shown is the median, upper and lower quartile, and with 99/1% whiskers for the four different fCa scenarios and three different slopes of degassing fractionation. The dashed green line gives the upper limit of calcite expected to form from dripwaters in the temperate conifer ecosystem; interglacial $\delta^{13}C_{init}$ not expected to be more negative than this value.

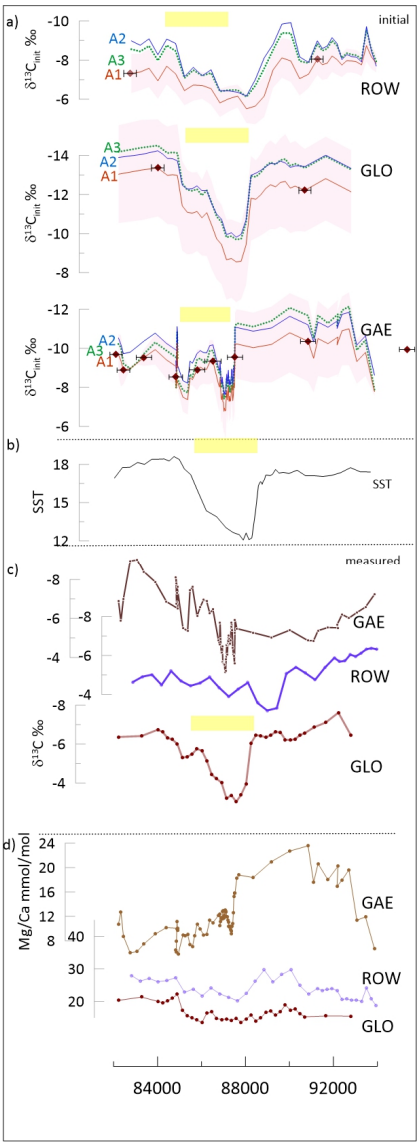
a)
initial
A2
A3
A1
ROW
GLO
GAE
δ13Cinit ‰
b)
SST
c)
measured
δ13C ‰
d)
Mg/Ca mmol/mol
84000
88000
92000

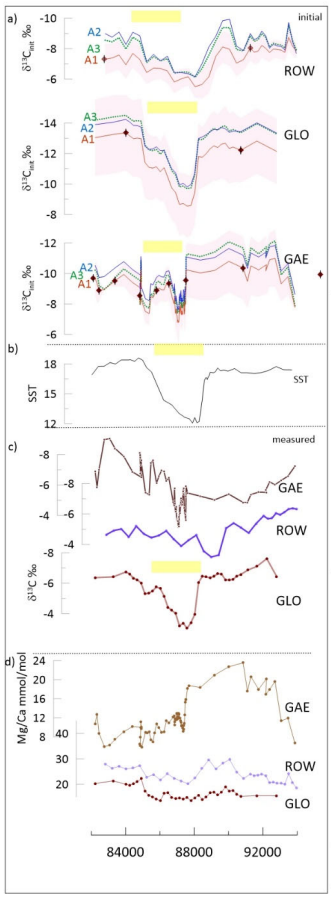
a)
initial
ROW
GLO
GAE
δ13Cinit ‰
b)
SST
c)
measured
δ13C ‰
d)
Mg/Ca mmol/mol
84000
88000
92000

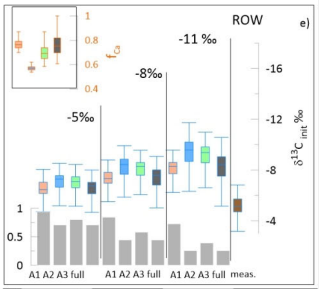
ROW
e)
-11 ‰
-8‰
-5‰
fcal3
δ13Cinit ‰
A1 A2 A3 full
A1 A2 A3 full
A1 A2 A3 full meas.

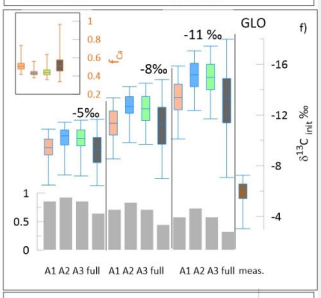
GLO
f)
-11 ‰
-8‰
-5‰
fcal3
δ13Cinit ‰
A1 A2 A3 full
A1 A2 A3 full
A1 A2 A3 full meas.

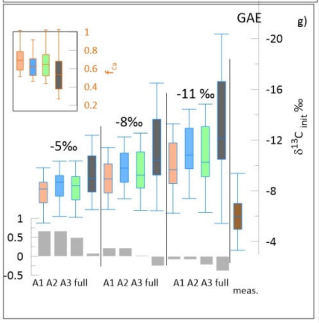
GAE
g)
-11 ‰
-8‰
-5‰
fcal3
δ13Cinit ‰
A1 A2 A3 full
A1 A2 A3 full
A1 A2 A3 full
meas.

Figure 7. Stadial event in time interval 94 to 82 ka in ROW, GLO, and GAE. a) for each stalagmite, the $\delta^{13}C_{init}$ for three fCa scenarios (A1, A2 solid lines, A3 dashed line); the line shows the result for degassing fractionation slope of -8 ‰, and shading for the A1 scenario shows the range using other degassing slopes of -5 ‰ (more positive), and -11 ‰ (more negative). Diamond symbols on the red curve indicate the position of U/Th dates and the uncertainty in the age. b) the SST record from the Iberian Margin (Martrat et al., 2007). c) the measured $\delta^{13}C$ for the three stalagmites, small symbols indicate measured samples. ~~d)~~ d) Mg/Ca for the three stalagmites, small symbols indicate measured samples~~. e) through g) inset shows the median and range of fCa for the various scenarios. Box and whisker plot shows the median, upper and lower quartile, and 1/99% ranges for the calculated $\delta^{13}C_{init}$ for each of the fCa scenarios (color coded as in Table 3 and Figure 5) and the measured $\delta^{13}C$. . Gray bars at the base of each figure illustrate the Pearson correlation coefficient between the $\delta^{13}C_{init}$ and the measured $\delta^{13}C_{init}$.~~ Box and whisker plot is given in Supplemental Figure 2. In a) through c), yellow bars highlight the inferred position of the stadial cooling event in each record, given uncertainty in age model.

~~**Figure 8. Glacial to Holocene transition in GUL with U/Th age control points illustrated along the age axis. a) the measured $\delta^{13}C$ for GUL. b) the $\delta^{13}C_{init}$ for three fCa scenarios; the line shows the result for degassing fractionation slope of -8 ‰, and shading for the A3 scenario shows the range using other degassing slopes of -5 ‰ (more positive), and -11 ‰ (more negative). c) the alkenone-based SST for the southern Iberian Margin(Cacho et al., 1999), d) the Mg/Ca for GUL. e) shows the median and range of fCa for the various scenarios. Box and whisker plot is given in Supplementary Figure 2. Green shading highlights the BA period.**~~

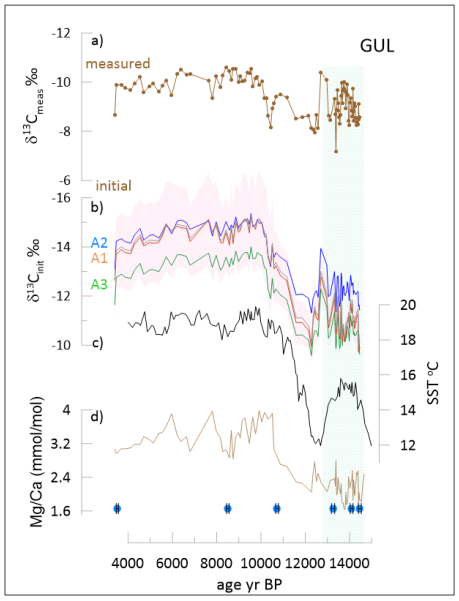

4.5.3 Deglaciation

For the Holocene stalagmite GUL, there is a significant temporal trend of Mg/Ca increase from the Bølling Allerød (B/A) into the Holocene (Figure 8; Supplemental Figure 3). Measured $\delta^{13}C$ was comparable in the B/A and the Holocene, but for all scenarios and degassing slopes, the $\delta^{13}C_{init}$ exhibits greater contrast between the early glacial and the Holocene, as the calculated $\delta^{13}C_{init}$ of the Bølling Allerød (B/A) is more positive than that of the Holocene. A similar steepening of the temporal trend in $\delta^{13}C_{init}$ occurs for stalagmite GLD spanning the penultimate deglaciation. GLD measured $\delta^{13}C$ features a very stable average value punctuated with two positive anomalies, while Mg/Ca exhibits a decrease over the deglaciation. The $\delta^{13}C_{init}$

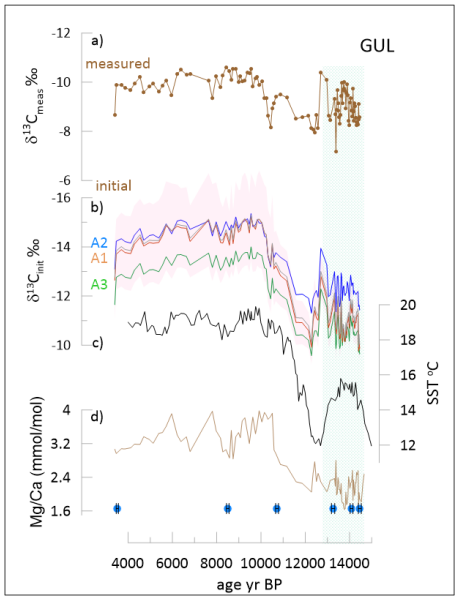

features a significant negative shift between 136 and 130 ka. With this significant change in trends among $\delta^{13}C_{init}$ and measured $\delta^{13}C$, correlation coefficients drop well below 0.5 for two scenarios at the -8 slope of degassing and correlations approach 0 at the -11‰ slope (Figure 9; Supplemental Figure 4).

Figure 8. Glacial to Holocene transition in GUL. a) the measured $\delta^{13}C$ for GUL. b) the $\delta^{13}C_{init}$ for three fCa scenarios; the line shows the result for degassing fractionation slope of -8 ‰, and shading for the A3 scenario shows the range using other degassing slopes of -5 ‰ (more positive), and -11 ‰ (more negative). c) the alkenone-based SST for the southern Iberian Margin(Cacho et al., 1999), d) the Mg/Ca for GUL. At the base the position of U/Th age points and their uncertainty are indicated with diamond symbols. Box and whisker plot is given in Supplemental Figure 3. Green shading highlights the BA period.

~~**Figure 9. Penultimate glacial to interglacial transition in GLD showing the measured $\delta^{13}C$ (brown curve with symbols indicating measured samples) and colored lines the $\delta^{13}C_{init}$ for three fCa scenarios A1, A2, and A3 (dashed line) for degassing fractionation slope of -8 ‰. Shading for the A3 scenario shows the range using other degassing slopes of -5 ‰ (more positive), and -11 ‰ (more negative). Mg/Ca also shown with solid brown line. Box and whisker plot is given in Supplementary Figure 4.**~~

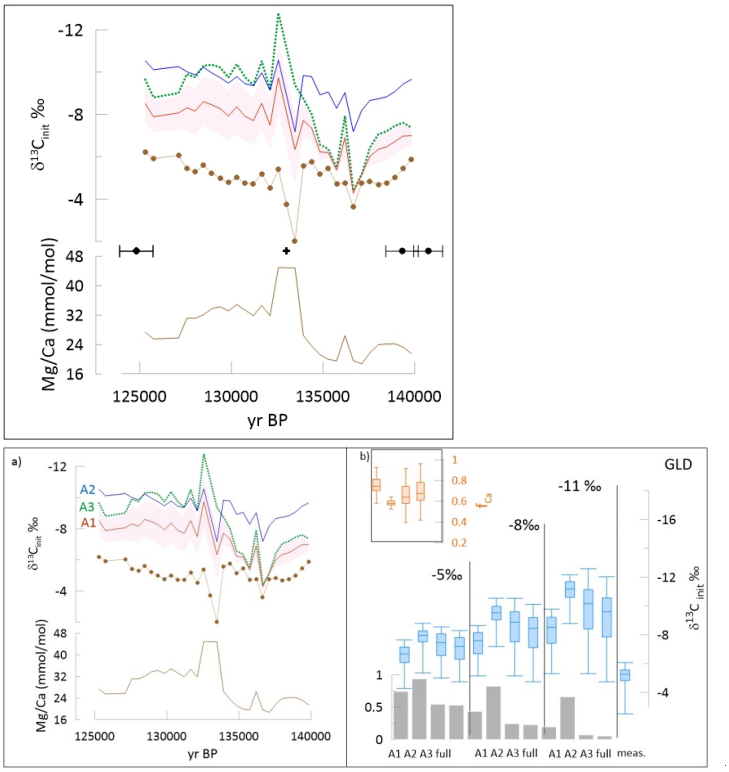

Figure 9. Penultimate glacial to interglacial transition in GLD showing the measured $\delta^{13}C$ (brown curve with symbols indicating measured samples) and colored lines the $\delta^{13}C_{init}$ for three fCa scenarios A1, A2, and A3 (dashed line) for degassing fractionation slope of -8 ‰. Shading for the A3 scenario shows the range using other degassing slopes of -5 ‰ (more positive), and -11 ‰ (more negative). Black diamonds indicate the position of U/Th dates and their uncertainty; the black cross indicates a tiepoint based on d18O as indicated in Supplemental Table 2. Mg/Ca also shown with solid brown line. Box and whisker plot is given in Supplemental Figure 4.

595

5. Discussion:

5.1 Interpretation of $\delta^{13}C_{init}$ and coherence of coeval speleothem signals and regional climate

The calculated $\delta^{13}C_{init}$ is formulated to reflect the isotopic signal of DIC prior to significant evolution via degassing and PCP. Warmer interglacial climates characterized by higher soil pCO_2 promote both more negative $\delta^{13}C_{DIC.}$ and increase the degree
600 of dripwater saturation which promotes greater PCP for a given drip interval (Fig. 4). For some locations with drip intervals very sensitive to PCP, these processes may exert comparable magnitude but opposing influence on measured stalagmite $\delta^{13}C$ and lead to nearly constant measured $\delta^{13}C$ despite significant changes in temperature(Martrat et al., 2007) and vegetation(Goni et al., 2008; Tzedakis et al., 2018). We suggest that such process may have contributed to the similar average measured $\delta^{13}C$ in GUL in late glacial and Holocene time intervals (Fig. 6), and also to the similar glacial and interglacial measured $\delta^{13}C$ in GLD (Fig 7). Both of these stalagmites are characterized by large increases in Mg/Ca in the interglacial, indicating significant enhancements of PCP.

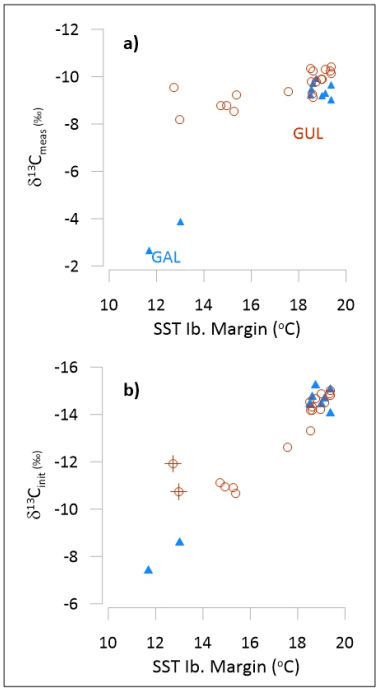

For stalagmite GUL growing during the last deglaciation, all of the examined calculations of $\delta^{13}C_{init}$ yield a temporal pattern more consistent with independent evidence for cooler regional temperatures during the late Glacial B/A compared to the early Holocene (Fig. 7) (Martrat et al., 2007; Ausín et al., 2019; Cacho et al., 1999). The aggregate $\delta^{13}C_{init}$ of both stalagmites spanning TI (GAL and GUL) exhibits a stronger correlation with regional SST than the measured $\delta^{13}C$ (Figure 10).

Figure 10. Comparison in 500 ky fixed time bins of a) measured $\delta^{13}C$ and b) $\delta^{13}C_{init}$ vs. regional Iberian Margin SST (Cacho et al., 1999) over the last glacial to interglacial transition in GAL (blue triangle) and GUL(red circle). In b) we show a -8 ‰ degassing slope and scenario A1. Other scenarios for GAL illustrated in Supplementary Figure 53. In lower panel, crosses denote two samples of age 12.25 and 12.75 ka, where offset may reflect uncertainty in the age interpolation as shown in Figure 8.

Because the extent of degassing and PCP can be strongly conditioned by the drip rate and drip chemistry supplying an
625 individual stalagmite, the extent and temporal variations of PCP may differ significantly among coeval stalagmites, leading to contrasting measured δ13C among coeval stalagmites even in the case of similar temperature and vegetation forcing of the initial dripwater $\delta^{13}C_{DIC}$. Between 94 and 82 ka, the Greenland Stadial (GS) 22 event is a salient cooling feature in regional

SST records(Martrat et al., 2007). Yet, only one of the three stalagmites spanning this age range exhibits a clear positive anomaly in measured $\delta^{13}C$, stalagmite GLO which features stable Mg/Ca over this time interval. Stalagmite GAE features a long term trend towards negative measured $\delta^{13}C$ not observed in GLO or ROW, and GAE features also a significant decrease in Mg/Ca (Fig. 7). The calculated $\delta^{13}C_{init}$ of GLO does not alter the trend seen in measured $\delta^{13}C$. However, the $\delta^{13}C_{init}$ of ROW features the positive anomaly typical for the stadial cooling. Significantly, despite the strong long term trend in measured $\delta^{13}C$, the calculated $\delta^{13}C_{init}$ of GAE also resolves a positive anomaly consistent with the timing of the GS22 cooling. These more coherent temporal trends are resolved in the three records regardless of the fCa scenario employed.

These results for multiple coeval stalagmites suggest that calculation of $\delta^{13}C_{init}$ has the potential to improve reproducibility among coeval records and resolve signals of important regional changes in temperature and vegetation effects in the soil and epikarst environment.

5.2 Coherency of quantitative PCP estimations and impact on deconvolving PCP effects in $\delta^{13}C$

5.2.1 Quantitative PCP indicators in this sample set

The calculation of $\delta^{13}C_{init}$ relies on quantitative estimation of PCP. PCP should exert a similar effect on ratios of divalent cations with low ~~partitioning~~partition coefficients like Mg/Ca and Sr/Ca. However, many published Mg/Ca and Sr/Ca records do not exhibit strong positive correlation(Sinclair, 2011). In our dataset, the greater correlation of Mg/Ca and Sr/Ca in some of the high Mg/Ca stalagmites may reflect the proportionally greater effect of calcite Mg/Ca on the D_{Sr} in higher Mg/Ca stalagmites (eg Wassenburg et al 2019). A threefold reduction in Ca due to PCP is attainable for reasonable degrees of soil pCO_2 and dripwater saturation in our interglacial climates, and therefore a threefold range in Mg/Ca or Sr/Ca due to PCP is possible. Over a threefold range in Mg/Ca in low Mg/Ca stalagmites (eg 2 to 6 mmol/mol Mg/Ca), existing compilations suggest that the D_{Sr} increases by 20%. Yet, for a 3-fold increase in Mg/Ca in the high Mg/Ca stalagmites (e.g. 10 to 30 mmol/mol Mg/Ca) the D_{Sr} would increase by 80%. Because Mg/Ca and $\delta^{44}Ca$ are always positively correlated, but Sr/Ca and $\delta^{44}Ca$ are not positively correlated in all samples, we conclude that growth rate-driven variations in D_{Sr} can strongly overprint the PCP-driven trends in Sr/Ca in some stalagmites. For a given fCa, faster growth rates would promote a lower $\delta^{44}Ca$ and a higher DSr, fueling inverse correlation. Because Ca and Sr are dominantly bedrock sourced in this setting, this reversal from PCP-expected relationship cannot be attributed to variable contribution of other element sources, but must reflect operation of processes at the solution-calcite interface. Similarly, deviation of Sr/Ca and Mg/Ca from the PCP slope, or variation in the Sr/Mg ratio does not conclusively require variation in non-bedrock sources in either element but could reflect ~~partitioning~~partitioning effects which for Sr are decoupled from PCP, as suggested by strong growth rate dependence of Sr partitioning in stalagmites from this cave(Sliwinski et al., 2023).

In our dataset, temperature variation in D_{Mg}~~DMg~~ could explain some, but not all of the apparent amplification in the Mg/Ca-based fCa compared to $\delta^{44}Ca$ -based fCa. Significant amplification is observed within the Holocene when temperature variation is limited. Additionally, in many cases the required range in D_{Mg}~~DMg~~ is larger than the 22% increase predicted from

reasonable (eg <10 degree) amplitude temperature increases according to laboratory calibrations(Day and Henderson, 2013). One candidate explanation for higher magnitude changes in D_{Mg}~~DMg~~ may be the up to 2-fold increase in the D_{Mg}~~DMg~~ with increasing calcite Mg/Ca (Wassenburg et al., 2020). This effective ~~partitioning~~partitioning increase may reflect true lattice ~~partitioning~~partitioning and/or increased Mg in fluid inclusions. The existing field data do not precisely constrain the slope of this increase in D_{Mg}~~DMg~~ or define if the slope is indeed linear. For future absolute estimation of fCa from Mg/Ca, improved constraints on the variation of D_{Mg}~~DMg~~ are required from laboratory and field studies. In field monitoring studies, true variation in D_{Mg}~~DMg~~ can be most accurately determined when observations adequately control for both the initial solution Mg/Ca and the integrated water Mg/Ca during calcite precipitation, which may be higher than the initial Mg/Ca if a significant extent of the Ca is precipitated on the stalagmite from each solution aliquot. Future field monitoring and farmed calcite studies should also evaluate whether calcite fabrics could provide independent evidence for variation in $D_{Mg,}$ since some stalagmites show relationship between fabrics and Sr partitioning (Frisia et al., 2022).

In addition to variation in D_{Mg}~~DMg~~, temporal changes in the Mg/Ca of undegassed dripwater could also contribute to discrepancies between fCa from δ^{44}Ca and Mg/Ca (e.g. the requirement for AF >1). We observe only a greater, never lesser, magnitude Mg/Ca change than that expected from changes in fCa alone. In the La Vallina cave system~~our cave system~~, dripwater monitoring ~~in La Vallina system~~ shows very constant dripwater Mg/Sr ratios seasonally despite order of magnitude changes in dripwater flow rates (Figure 12 in (Kost et al., 2023) ~~(Kost et al., in review)~~. This suggests that despite variation in water residence times, there is not widespread or significant variation in bedrock mixing fraction~~significant variation in the congruency of bedrock dissolution is not pervasive despite variation in water residence times~~.

5.2.2 Suggested approach for fossil stalagmites

Mg/Ca is a widely measured PCP-sensitive indicator. However, it ~~but~~ can be unreliable in host rocks which feature significant components of widely varying solubility and Mg/Ca if the bedrock mixing fraction varies over time. This can ~~which~~produce ~~give rise to~~ variation in the initial dripwater Mg/Ca attained by bedrock dissolution before evolution of dripwater by PCP. ~~strong incongruency of dissolution.~~ Large temporal variations in dripwater Mg/Sr ratios at a single drip during monitoring may be one sign of varying bedrock mixing fraction~~such incongruency~~. Mg/Ca can also be unreliable as a PCP indicator if a large fraction of the Mg in the stalagmite is present in detrital minerals rather than in the calcite. Stalagmite Mg/Ca which covaries with Al/Ca or Si/Ca may indicate important detrital component of Mg. In these two situations, it is not recommended to use Mg/Ca for quantitative PCP estimation.

In settings where ~~congruency~~bedrock mixing fraction is ~~is expected~~stable and detrital minerals are not a significant source of Mg in the stalagmite, the quantitative estimation of fCa nonetheless entails uncertainty. For stalagmites in which only Mg/Ca is measured, and δ^{44}Ca is not determined, the constancy or range of variation in D_{Mg}~~DMg~~ will represent one source of uncertainty in the calculation of $\delta^{13}C_{init}$. The calculation of fCa from Mg/Ca can be adjusted by an attenuation factor as in Equation 7. An attenuation factor >1 is likely required if measured Mg/Ca leads to calculation of a larger fCa range than

expected. For example, an fCa <0.20 would require initial dripwater Ca concentrations > 100 ppm. If a bedrock adjustment factor in Equation 7 is used, it may need to be coupled with an attenuation factor (other than 1) so that absolute fCa does not reach values lower than expected for the cave and climatic context. This uncertainty will be reduced as future research better constrains the variation of D_{Mg} ~~DMg~~ with Mg/Ca.

5.3 What is the magnitude of PCP+degassing effect on $\delta^{13}C$?

5.3.1 Do interglacial stalagmites constrain the degassing $\delta^{13}C$ slope?

For interglacial stalagmites, we can estimate the lowest expected $\delta^{13}C_{init}$ and use this limit to evaluate the range of reasonable degassing slopes. The $\delta^{13}C_{DIC}$ of dripwater has been measured under forested sections of the cave, with sample collection techniques to limit degassing(Kost et al., 2023) ~~(Kost et al., in review)~~. From this, we estimate the $\delta^{13}C_{init}$ for calcite forming under similar dripwater $\delta^{13}C_{DIC.}$ Additionally, we hypothesize that pre-anthropogenic land use at this location would have led to soil pCO_2 in the 8,000 to 10,000 ppm range during the mid-Holocene and previous interglacials(Lechleitner et al., 2021a). We therefore calculate the composition of calcite forming from DIC in equilibrium with open system dissolution (eg 150 L gas volume and resulting 3% dcp) of limestone by 10000 ppm soil CO_2 of isotopic composition corresponding to modern respired endmembers in three ecosystems(Pataki et al., 2003)(Figure 6).

We find that interglacial stalagmites cannot rule out any of the investigated degassing slopes. The stalagmites from our monitored cave which include long Holocene growth phases are GAL and GUL, which require low to moderate attenuation factors (1.3 to 3) for calculation of fCa from Mg/Ca. When the fCa calculated from Mg/Ca include the estimated AF for coherency with $\delta^{44}Ca$ as in Table 2~~3~~, then the -8 ‰ slope for all GUL and GAL samples fall within the range of calcite composition expected from modern dripwater with limited degassing (Fig. 6). With the -11‰ slope, the median $\delta^{13}C_{init}$ approaches -17‰, which albeit higher than modern dripwater predictions, is still compatible with DIC deriving from equilibration with respired CO_2 from temperate broadleaf and conifer ecosystems(Pataki et al., 2003). With the -5‰ slope, the median $\delta^{13}C_{init}$ is slightly below that implied for calcite on the basis of modern monitoring. Results for stalagmites spanning the last interglacial also indicate that the -8 to -11‰ slopes yield $\delta^{13}C_{init}$ coherent with expected interglacial calcite. BEL, which requires little attenuation, best matches expected range with the -11‰. But, our comparison does reveal that unreasonable corrections which are more negative than expected for the respired CO_2 component result from the combination of -11‰ degassing slope and fCa calculated from measured Mg/Ca without use of AF (scenario “full”), for some low Mg/Ca stalagmites.

A similar analysis for the Holocene Heshang Cave, for which both Mg/Ca and fCa data are available, yields $\delta^{13}C_{init}$ with the -5‰ slope of -12‰ and with the -11‰ slope $\delta^{13}C_{init}$ of -15‰, both within the range of calcite composition expected from high CO_2 soils with respired CO_2 composition from temperature broadleaf or tropical ecosystems(Pataki et al., 2003) (Figure 6), consistent with the C3 evergreen broadleaf vegetation overlying Heshang Cave(Li et al., 2014).

Thus, the available interglacial datasets so far do not preclude the kinetically-enhanced slope of -11‰ for fractionation during degassing and PCP. In fact, for the last interglacial, for many stalagmites, the higher slopes yield $\delta^{13}C_{init}$ more consistent expected interglacial soil pCO_2. Although the degree of open vs closed dissolution cannot be inferred for last interglacial samples, if it is in the range of Holocene and late glacial samples from this and nearby caves (Lechleitner et al., 2021b), the $\delta^{13}C_{init}$ is not expected to differ by more than (1‰) from that calculated for the relatively open 10000 ppm soil CO_2 CaveCalc model.

5.3.2 Previous laboratory and field calibrations

The CaveCalc simulation assumes that the loss of carbon from dripwater is attained via CO_2 degassing and calcite precipitation in a 1:1 ratio, with close coupling of the processes, and that fractionation is occurring at equilibrium according to laboratory-estimated fractionation factors.

Empirical laboratory and field results are sensitive to true degassing and PCP as well as the isotopic consequences of exchange between dripwater and cave atmosphere.

We are aware of one published field study in which dripwater was sampled before and after a ~3 m transit across a subvertical flowstone surface in a cave with average temperature of 22.5°C (Mickler et al., 2019). In this transect, Ca and DIC were directly measured and $\delta^{13}C$ DIC was determined from total evolution as CO_2 in flushed vials. Ca concentrations were on average 20% lower after the ISST flowstone transit, and the median estimated degassing slope was -9.9‰ in the 8 monthly paired samples. The slopes estimated on individual sampling dates (ranging from -7.7 to -13.7) did not correlate with dripwater oversaturation nor the estimated ratio of Ca to DIC decrease on those dates. The slope in this study is more than double that of CaveCalc at comparable temperatures. One interpretation is that the rapid initial phases of degassing occur at kinetically-enhanced fractionation factors (Mickler et al., 2019). A similar experiment conducted on one day in La Vallina Cave was also consistent with a slope of -11‰, based on sampling during cave temperature of at 12°C and modest saturation (55 ppm Ca in dripwater, vs 21 ppm for equilibrium at cave temperature and pCO_2 ppm)(Kost et al., 2023)~~, (Kost et al., In review)~~. During this sampling, cave air was ventilated to near atmospheric CO_2 concentrations and isotopic composition. These laboratory and field results suggest that, given current available data, the CaveCalc slopes may need to be considered the minimum slopes required to correct for degassing and PCP effects on carbon isotopes.

The laboratory experiment best simulating the coupled evolution of $\delta^{13}C$ DIC, calcite $\delta^{13}C$ and fCa allowed highly supersaturated solutions to degas and precipitate $CaCO_3$ as they flowed along a marble plate, with electrical conductivity measurements estimating the degree of Ca depletion along the flow path in a parallel experimental setup with flow over a glass plate (Hansen et al., 2019). The $\delta^{13}C$ of DIC was measured by precipitation in $SrCO_3$ and analysis as solid phase. The slope A in the 10 experiments, based on the evolution of $\delta^{13}C$ of DIC, ranged from -4.63 to -13.2‰, or from -5.9 to -16‰ based on evolution of $\delta^{13}C$ of calcite, although precise estimation of the latter slope is complicated by the measurement of precipitated calcite $\delta^{13}C$ and conductivity in separate experimental setups which may have experienced slightly different locations of

calcite precipitation(Sade et al., 2022). Many of these estimated experimental fractionations are considerably higher than those predicted by CaveCalc.

A dynamical model (Sade et al., 2022) was developed to simulate the laboratory experiments(Hansen et al., 2019). This model derived a single relationship between PCP and DIC evolution, using fDIC in contrast to our calculated index based on Ca comsumption, fCa. In this model formulation, the degassing slope relative to ln (fDIC) averages -8.7 ‰ from f=1.0 to f=0.3, but the slope is not constant. Rather, at fDIC between 0.8 and 1, there is an inverse slope as net DIC evolution is modelled to lead to more negative, rather than more positive, $\delta^{13}C$ of speleothem calcite. Over the subsequent phase of PCP (fDIC 0.8 to 0.3), the average modelled degassing slope relative to fDIC would be -10.1‰, however it flattens to -4‰ in the range of fDIC 0.33 to 0.4. If this model is representative of cave flowstone formation, it may suggest that some of the calculated differences in degassing slopes in field experiments may result from measurements of solutions sampled in different stages of dripwater Ca and DIC evolution. Alternatively, it is possible that some differences in degassing slopes reflect different degrees of coupling between degassing and $CaCO_3$ precipitation. The influence of factors inhibiting $CaCO_3$ precipitation, potentially including elevated Mg concentrations or certain dissolved organic compounds, on the degassing slope remains to be investigated.

If there were significant variations in the degassing slope experienced by a given stalagmite over time, it could complicate efforts to estimate trends in $\boldsymbol{\delta}^{13}C_{init}$ using Eqn. 2. Yet, our speleothem time series are broadly consistent with narrow range of variation of degassing slope within a given stalagmite, since correction of -5 ‰ in one part of the time series and -11‰ in another would alter the trends and reduce coherence among the records in Figure 7. This coherence with a single slope may reflect the limited range of variation in fCa inferred for our stalagmites. For example, for all stalagmites except GAE, the A2 scenarios, and the majority of data from A3 scenarios, fall between fCa of 0.4 and 0.8. If coincident with fDIC of 0.4 to 0.8, these samples would all be within the range of similar slope (-10 to -11.5‰) predicted by the dynamical model simulation. Sampled stalagmite growth may often be biased to periods when fCa >0.4, which lead to higher precipitation rates and more calcite deposition. The consistency of our interglacial data with steeper degassing slopes than CaveCalc may reflect the reality that much calcite precipitation will happen when cave pCO_2 is much lower than dripwater pCO_2, a situation in which dripwater exchange with isotopically heavier cave air could be significant contributor to a steep degassing slope.

A future calculation of the dynamical model prediction(Sade et al., 2022) of $\delta^{13}C$ evolution relative to fCa, rather than fDIC, as a PCP indicator, would provide a helpful reference to future calculation of $\boldsymbol{\delta}^{13}C_{init.}$ This could elucidate whether a nonlinear relationship should be used to calculate $\boldsymbol{\delta}^{13}C_{init}$ from ln (fCa) and $\boldsymbol{\delta}^{13}C_{meas}$. It would clarify if calcite precipitated at high fCa, analogous to that precipitated at high fDIC, should be excluded from the correction because of compensating effects of kinetic fractionation factors and evolution of fCa in the range of high fCa. Scenarios employing a B $\leq$0.8 by default have a maximum fCa largely outside the range of inverse slope.

5.3.3 Suggested approach

Trends in $\delta^{13}C_{init}$ are less sensitive to the choice of the degassing slope but the absolute value of $\delta^{13}C_{init}$ is strongly dependent on the choice of degassing slope. At the moment, the absolute $\delta^{13}C_{init}$ can be reconstructed with low confidence. However, the reconstructed $\delta^{13}C_{init}$ can be used to rule out combinations of fCa scenarios and degassing slopes which lead to "overcorrection" to $\delta^{13}C_{init}$ values which are more negative than DIC equilibrated with a reasonable respired soil pCO_2 composition for the ecosystem type. Until further constraints to assess the slope of $\delta^{13}C$ and Ca co-evolution during degassing and PCP which characterizes typical cave environments are available, a sensitivity analysis employing a range of degassing slopes will provide the greatest transparency for assessing $\delta^{13}C_{init.}$

6. Conclusions

We provide a first analysis of the potential estimation of speleothem $\delta^{13}C_{init,}$ the $\delta^{13}C$ which characterized dripwater DIC prior to significant degassing and PCP. $\delta^{13}C_{init}$ is proposed as a useful interpretable variable derived from speleothem isotope measurements, because trends in $\delta^{13}C_{init}$ are expected to be more reproducible than measured $\delta^{13}C$ among coeval stalagmites from a given region and because $\delta^{13}C_{init}$ is more sensitive to the vegetation, soil, and epikarst processes which in many regions may be sensitive to temperature in addition to moisture. Calculation of $\delta^{13}C_{init}$ for a given sample or growth increment requires a quantitative indicator of the extent of PCP experienced in that growth increment , and knowledge of the general rate of change of $\delta^{13}C$ with progressive degassing and PCP.

In fossil stalagmites, the extent of PCP, as the Rayleigh fCa, can be approximated for a particular growth increment using the measured Mg/Ca and the minimum Mg/Ca measured in the entire stalagmite. fCa can also be estimated from $\delta^{44}Ca$ given reasonable choices of the calcite-dissolved fractionation factor. In several of the stalagmites examined here, the fCa calculated from Mg/Ca shows an amplified range compared to that calculated from $\delta^{44}Ca$. An increase in D_{Mg}~~DMg~~ with increasing Mg/Ca, as proposed in previous studies (Wassenburg et al., 2020), is one viable explanation for this systematic trend. This observation warrants further investigation to improve confidence in future estimates of fCa from Mg/Ca, which is the most widely available PCP indicator for stalagmites.

At the moment, there is uncertainty in the degassing slope or rate of change of $\delta^{13}C$ with progressive degassing and PCP. Values may range from -5 to -11‰. The stalagmites investigated here could be consistent with any value in this range. Because these different possible degassing slopes affect the absolute value of the calculate $\delta^{13}C_{init,}$ currently there is uncertainty in exact value. However, the trends in $\delta^{13}C_{init}$ are less sensitive to the choice of degassing slope.

Despite these uncertainties, $\delta^{13}C_{init}$ provides more consistent time series among coeval stalagmites and with regional climate records. In one example $\delta^{13}C_{init}$ reconciles three divergent measured stalagmite $\delta^{13}C$ records in the 94 to 82 ka time interval, yielding three $\delta^{13}C_{init}$ time series which feature a pronounced positive anomaly corresponding to the regional cooling of

Greenland Stadial 22. In Western Europe, over the warming trend of deglaciations, the trend towards more negative $\delta^{13}C_{DIC}$ due to higher soil respiration and soil CO_2 may be fully or partially compensated in stalagmite $\delta^{13}C$ due to the increased PCP from the more oversaturated dripwaters. The calculation of $\delta^{13}C_{init}$ reveals the trend of increasing respiration rates and soil pCO_2. Over the last deglaciation, the $\delta^{13}C_{init}$ matches millennial structure in regional SST more closely than the measured $\delta^{13}C$.

As better constraints emerge on the degassing slope and on Mg partitioning, $\delta^{13}C_{init}$ estimates will become more precise and should improve the utility of the high volume of stalagmite $\delta^{13}C$ measurements made simultaneous with $\delta^{18}O$ in all labs.

Appendix A. Measured $\delta^{44}Ca$, Mg/Ca and Sr/Ca, and the calculated fCa for differing $\Delta^{44}Ca$, and B (bedrock factors).

				fCa from $\delta^{44}Ca$				fCa from Mg/Ca			fCa from Sr/Ca		
				Δ44Ca ‰				B			B		
	$\delta^{44/40}Ca$ ‰	Mg/Ca (mmol/mol)	Sr/Ca (mmol/mol)	*-0.66*	*-0.86*	*-1.08*	*-1.37*	1	0.8	0.6	1	0.8	0.6
GAL-37.5	0.21	3.12	0.034	0.64	0.56	0.52	0.48	0.35	0.28	0.21	0.69	0.55	0.41
GAL-42	0.19	2.78	0.035	0.66	0.58	0.53	0.49	0.39	0.31	0.24	0.66	0.53	0.40
GAL 42.5	0.12	1.79	0.035	0.74	0.63	0.562	0.51	0.61	0.49	0.36	0.67	0.53	0.40
Gal 16	0.06	1.57	0.040	0.80	0.67	0.59	0.54	0.70	0.56	0.42	0.57	0.46	0.34
Gal 30	0.14	2.67	0.032	0.72	0.61	0.553	0.51	0.41	0.33	0.25	0.73	0.58	0.44
Row 452	0.04	19.06	0.105	0.84	0.69	0.61	0.55	0.95	0.76	0.57	0.90	0.72	0.54
Row 252	0.12	26.58	0.129	0.73	0.63	0.56	0.51	0.68	0.54	0.41	0.74	0.59	0.44
BEL mid 210	-0.40	9.56	0.109	1.62	1.15	0.91	0.75	0.95	0.76	0.57	0.69	0.56	0.42
BEL mid 60	-0.13	14.52	0.130	1.08	0.84	0.71	0.62	0.62	0.50	0.37	0.58	0.46	0.35
GAE_33.5 nd	-0.41	4.39	0.109	1.66	1.17	0.92	0.76	0.49	0.39	0.29	0.23	0.18	0.14
GAE_60.4 nd	0.13	17.59	0.115	0.73	0.62	0.56	0.51	0.12	0.10	0.07	0.22	0.17	0.13
GAR_b2_035.0	-0.25	7.42	0.097	1.29	0.96	0.79	0.67	0.33	0.26	0.20	0.29	0.23	0.17
GAR_b6_131.5	-0.49	2.42	0.073	1.85	1.27	0.99	0.80	1.00	0.80	0.60	0.39	0.31	0.23
GLO_b1_17.4	0.23	9.74	0.037	0.63	0.55	0.51	0.48	0.78	0.62	0.47	0.55	0.44	0.33
GLO_b2_08.2	0.42	17.24	0.068	0.47	0.44	0.43	0.41	0.44	0.35	0.26	0.30	0.24	0.18
GUL4-2.3	-0.15	2.19	0.062	1.11	0.86	0.72	0.63	0.74	0.59	0.45	0.41	0.33	0.25
GUL_I-3	0.06	3.69	0.033	0.81	0.67	0.60	0.54	0.44	0.35	0.27	0.78	0.62	0.47
NYM_331	-0.13	11.29	0.119	1.08	0.84	0.71	0.62	0.82	0.66	0.49	0.74	0.59	0.45
NYM_457.5	-0.04	13.67	0.134	0.94	0.75	0.65	0.58	0.85	0.68	0.51	0.69	0.56	0.42

Data availability.

Data and sample excel for calculations are archived in the ETH Research Collection at doi: 10.3929/ethz-b-000630754. ~~Upon acceptance, data will be archived on the ETH data repository on the SISAL template, and presented for inclusion in the subsequent version of SISAL~~.

Supplementary file accompanies this manuscript.

Author contributions. HMS conceived the study, conducted calculations, prepared figures and wrote the text with discussions from CD and FL. CD completed Ca isotope measurements. FL and LE conducted CaveCalc simulations. OK and JS assisted with trace element analysis and sampling for Ca isotopes and dating. DS contributed to interpretation. HC and CP completed new chronology.

Competing interests.

The authors declare they have no conflict of interest.

Acknowledgments

HS acknowledges ETH core funding and grant ETH-13 18-1. FL was supported by SNSF grant P400P2_180789. CD and Ca-isotope measurements were supported with funds from John Fell Oxford University Press Research Fund grant 0007911. FL was supported by SNSF grant P400P2_180789. CP and HC acknowledge NSFC (41888101, 42050410317) and Postdoctoral Science Foundation of China (2020M683452). We thank ETH Climate Geology lab manager Madalina Jaggi and student assistants Tim Loeffel and Romain Alosius for assistance with stable isotope and trace element sampling. We thank the ETH fall 2021 Paleoclimate course students and course assistant Pien Anjewierden for preparing samples from GLD, and Fall 2019 Paleoclimate course students for initiating study of GUL.

References

Alkhatib, M., Qutob, M., Alkhatib, S., and Eisenhauer, A.: Influence of precipitation rate and temperature on the partitioning of magnesium and strontium in calcite overgrowths, Chemical Geology, 599, 120841, 2022.

Ausín, B., Magill, C., Haghipour, N., Fernández, Á., Wacker, L., Hodell, D., Baumann, K.-H., and Eglinton, T. I.: (In) coherent multiproxy signals in marine sediments: Implications for high-resolution paleoclimate reconstruction, Earth and Planetary Science Letters, 515, 38-46, 2019.

Breitenbach, S. F. and Bernasconi, S. M.: Carbon and oxygen isotope analysis of small carbonate samples (20 to 100 µg) with a GasBench II preparation device, Rapid Communications in Mass Spectrometry, 25, 1910-1914, 2011.

Cacho, I., Grimalt, J. O., Pelejero, C., Canals, M., Sierro, F. J., Flores, J. A., and Shackleton, N.: Dansgaard-Oeschger and Heinrich event imprints in Alboran Sea paleotemperatures, Paleoceanography, 14, 698-705, 1999.

Day, C. C. and Henderson, G. M.: Controls on trace-element partitioning in cave-analogue calcite, Geochimica et Cosmochimica Acta, 120, 612-627, 2013.

de Wet, C. B., Erhardt, A. M., Sharp, W. D., Marks, N. E., Bradbury, H. J., Turchyn, A. V., Xu, Y., and Oster, J. L.: Semiquantitative estimates of rainfall variability during the 8.2 kyr event in California using speleothem calcium isotope ratios, Geophysical Research Letters, 48, e2020GL089154, 2021.

Formatted: English (United States)

DePaolo, D. J.: Surface kinetic model for isotopic and trace element fractionation during precipitation of calcite from aqueous solutions, Geochimica et Cosmochimica Acta, 75, 1039-1056, http://dx.doi.org/10.1016/j.gca.2010.11.020, 2011.

Dorale, J. A. and Liu, Z.: Limitations of Hendy test criteria in judging the paleoclimatic suitability of speleothems and the need for replication, Journal of Cave and Karst Studies, 71, 73-80, 2009.

Emrich, K., Ehhalt, D., and Vogel, J.: Carbon isotope fractionation during the precipitation of calcium carbonate, Earth and Planetary Science Letters, 8, 363-371, 1970.

Fairchild, I. J. and Treble, P. C.: Trace elements in speleothems as recorders of environmental change, Quaternary Science Reviews, 28, 449-468, 2009.

Frisia, S., Borsato, A., Hartland, A., Faraji, M., Demeny, A., Drysdale, R. N., and Marjo, C. E.: Crystallization pathways, fabrics and the capture of climate proxies in speleothems: Examples from the tropics, Quaternary Science Reviews, 297, 107833, 2022.

Genty, D., Blamart, D., Ouahdi, R., Gilmour, M., Baker, A., Jouzel, J., and Van-Exter, S.: Precise dating of Dansgaard–Oeschger climate oscillations in western Europe from stalagmite data, Nature, 421, 833-837, 2003.

Genty, D., Blamart, D., Ghaleb, B., Plagnes, V., Causse, C., Bakalowicz, M., Zouari, K., Chkir, N., Hellstrom, J., and Wainer, K.: Timing and dynamics of the last deglaciation from European and North African δ13C stalagmite profiles—comparison with Chinese and South Hemisphere stalagmites, Quaternary Science Reviews, 25, 2118-2142, 2006.

Goni, M. F. S., Landais, A., Fletcher, W. J., Naughton, F., Desprat, S., and Duprat, J.: Contrasting impacts of Dansgaard–Oeschger events over a western European latitudinal transect modulated by orbital parameters, Quaternary Science Reviews, 27, 1136-1151, 2008.

Hansen, M., Scholz, D., Schöne, B. R., and Spötl, C.: Simulating speleothem growth in the laboratory: Determination of the stable isotope fractionation (δ13C and δ18O) between H2O, DIC and CaCO3, Chemical Geology, 509, 20-44, 2019.

Hansen, M., Scholz, D., Froeschmann, M.-L., Schöne, B. R., and Spötl, C.: Carbon isotope exchange between gaseous CO2 and thin solution films: Artificial cave experiments and a complete diffusion-reaction model, Geochimica et Cosmochimica Acta, 211, 28-47, 2017.

Hendy, C. H.: The isotopic geochemistry of speleothems—I. The calculation of the effects of different modes of formation on the isotopic composition of speleothems and their applicability as palaeoclimatic indicators, Geochimica et Cosmochimica Acta, 35, 801-824, http://dx.doi.org/10.1016/0016-7037(71)90127-X, 1971.

Hippler, D., Schmitt, A. D., Gussone, N., Heuser, A., Stille, P., Eisenhauer, A., and Nägler, T. F.: Calcium isotopic composition of various reference materials and seawater, Geostandards Newsletter, 27, 13-19, 2003.

Hofmann, A. E., Bourg, I. C., and DePaolo, D. J.: Ion desolvation as a mechanism for kinetic isotope fractionation in aqueous systems, Proceedings of the National Academy of Sciences, 109, 18689-18694, 2012.

Kost, O., Sliwinski, J., Gies, N., Lueder, M., and Stoll, H. M.: The influence of fluid inclusions, organics, and calcite fabric on trace element distributions in stalagmites, Frontiers in Earth Science, in review.

Kost, O., Gonzalez Lemos, S., Rodriguez-Rodriguez, L., Sliwinski, J., Endres, L., Haghipour, N., and Stoll, H. M.: Relationship of seasonal variations in drip water δ13CDIC, δ18O, and trace elements with surface and physical cave conditions of La Vallina cave, NW Spain, Hydrol. Earth Syst. Sci., 27, 2227-2255, https://doi.org/10.5194/hess-27-2227-2023, 2023.

Lechleitner, F. A., Day, C. C., Kost, O., Wilhelm, M., Haghipour, N., Henderson, G. M., and Stoll, H. M.: Stalagmite carbon isotopes suggest deglacial increase in soil respiration in Western Europe driven by temperature change, Climate of the Past, 17, 1903-1918, 2021a.

Lechleitner, F. A., Day, C. C., Kost, O., Wilhelm, M., Haghipour, N., Henderson, G. M., and Stoll, H. M.: Stalagmite carbon isotopes suggest deglacial increase in soil respiration in Western Europe driven by temperature change, Climate of the Past Discussions, 1-25, 2021b.

Li, X., Cui, X., He, D., Liao, J., and Hu, C.: Evaluation of the Heshang Cave stalagmite calcium isotope composition as a paleohydrologic proxy by comparison with the instrumental precipitation record, Scientific reports, 8, 1-7, 2018.

Li, X., Hu, C., Huang, J., Xie, S., and Baker, A.: A 9000-year carbon isotopic record of acid-soluble organic matter in a stalagmite from Heshang Cave, central China: Paleoclimate implications, Chemical Geology, 388, 71-77, 2014.

Lorens, R. B.: Sr, Cd, Mn and Co distribution coefficients in calcite as a function of calcite precipitation rate, Geochimica et Cosmochimica Acta, 45, 553-561, 1981.

Formatted: English (United States)

Formatted: English (United States)

Formatted: English (United States)

Formatted: English (United States)

Formatted: English (United States)

Magiera, M., Lechleitner, F. A., Erhardt, A. M., Hartland, A., Kwiecien, O., Cheng, H., Bradbury, H. J., Turchyn, A. V., Riechelmann, S., and Edwards, L.: Local and regional Indian summer monsoon precipitation dynamics during Termination II and the Last Interglacial, Geophysical Research Letters, 46, 12454-12463, 2019.
Martrat, B., Grimalt, J. O., Shackleton, N. J., de Abreu, L., Hutterli, M. A., and Stocker, T. F.: Four climate cycles of recurring deep and surface water destabilizations on the Iberian margin, Science, 317, 502-507, 2007.
Meyer, K. W., Feng, W., Breecker, D. O., Banner, J. L., and Guilfoyle, A.: Interpretation of speleothem calcite δ13C variations: Evidence from monitoring soil CO2, drip water, and modern speleothem calcite in central Texas, Geochimica et Cosmochimica Acta, 142, 281-298, 2014.
Mickler, P. J., Stern, L. A., and Banner, J. L.: Large kinetic isotope effects in modern speleothems, Geological Society of America Bulletin, 118, 65-81, 2006.
Mickler, P. J., Banner, J. L., Stern, L., Asmerom, Y., Edwards, R. L., and Ito, E.: Stable isotope variations in modern tropical speleothems: evaluating equilibrium vs. kinetic isotope effects, Geochimica et Cosmochimica Acta, 68, 4381-4393, 2004.
Mickler, P. J., Carlson, P., Banner, J. L., Breecker, D. O., Stern, L., and Guilfoyle, A.: Quantifying carbon isotope disequilibrium during in-cave evolution of drip water along discreet flow paths, Geochimica et Cosmochimica Acta, 244, 182-196, 2019.
Mills, J. V., DePaolo, D. J., and Lammers, L. N.: The influence of Ca: CO3 stoichiometry on Ca isotope fractionation: Implications for process-based models of calcite growth, Geochimica et Cosmochimica Acta, 298, 87-111, 2021.
Mook, W. and Rozanski, K.: Environmental isotopes in the hydrological cycle, Principles and Applications, Volumes I, IV and V, 2000.
Mucci, A. and Morse, J. W.: The incorporation of Mg2+ and Sr2+ into calcite overgrowths: influences of growth rate and solution composition, Geochimica et Cosmochimica Acta, 47, 217-233, 1983.
Mühlinghaus, C., Scholz, D., and Mangini, A.: Modelling stalagmite growth and δ13C as a function of drip interval and temperature, Geochimica et Cosmochimica Acta, 71, 2780-2790, 2007.
Mühlinghaus, C., Scholz, D., and Mangini, A.: Modelling fractionation of stable isotopes in stalagmites, Geochimica et Cosmochimica Acta, 73, 7275-7289, 2009.
Nielsen, L. C., De Yoreo, J. J., and DePaolo, D. J.: General model for calcite growth kinetics in the presence of impurity ions, Geochimica et Cosmochimica Acta, 115, 100-114, 2013.
Noronha, A. L., Johnson, K. R., Hu, C., Ruan, J., Southon, J. R., and Ferguson, J. E.: Assessing influences on speleothem dead carbon variability over the Holocene: implications for speleothem-based radiocarbon calibration, Earth and Planetary Science Letters
394, 20-29, 2014.
Owen, R., Day, C. C., and Henderson, G. M.: CaveCalc: A new model for speleothem chemistry & isotopes, Computers & Geosciences, 119, 115-122, 2018.
Owen, R., Day, C., Hu, C.-Y., Liu, Y.-H., Pointing, M., Blättler, C., and Henderson, G.: Calcium isotopes in caves as a proxy for aridity: Modern calibration and application to the 8.2 kyr event, Earth and Planetary Science Letters, 443, 129-138, 2016.
Pataki, D., Ehleringer, J., Flanagan, L., Yakir, D., Bowling, D., Still, C., Buchmann, N., Kaplan, J. O., and Berry, J.: The application and interpretation of Keeling plots in terrestrial carbon cycle research, Global biogeochemical cycles, 17, 2003.
Polag, D., Scholz, D., Mühlinghaus, C., Spötl, C., Schröder-Ritzrau, A., Segl, M., and Mangini, A.: Stable isotope fractionation in speleothems: Laboratory experiments, Chemical Geology, 279, 31-39, http://dx.doi.org/10.1016/j.chemgeo.2010.09.016, 2010.
Reynard, L., Day, C., and Henderson, G.: Large fractionation of calcium isotopes during cave-analogue calcium carbonate growth, Geochimica et cosmochimica acta, 75, 3726-3740, 2011.
Romanek, C. S., Grossman, E. L., and Morse, J. W.: Carbon isotopic fractionation in synthetic aragonite and calcite: effects of temperature and precipitation rate, Geochimica et cosmochimica acta, 56, 419-430, 1992.
Romanov, D., Kaufmann, G., and Dreybrodt, W.: Modeling stalagmite growth by first principles of chemistry and physics of calcite precipitation, Geochimica et Cosmochimica Acta, 72, 423-437, 2008.
Romero-Mujalli, G., Hartmann, J., Börker, J., Gaillardet, J., and Calmels, D.: Ecosystem controlled soil-rock pCO2 and carbonate weathering–Constraints by temperature and soil water content, Chemical Geology, 527, 118634, 2019.
Rubinson, M. and Clayton, R. N.: Carbon-13 fractionation between aragonite and calcite, Geochimica et Cosmochimica Acta, 33, 997-1002, 1969.

Formatted: English (United States)

Formatted: English (United States)

Sade, Z., Hegyi, S., Hansen, M., Scholz, D., and Halevy, I.: The effects of drip rate and geometry on the isotopic composition of speleothems: Evaluation with an advection-diffusion-reaction model, Geochimica et Cosmochimica Acta, 317, 409-432, 2022.
Scholz, D., Mühlinghaus, C., and Mangini, A.: Modelling δ13C and δ18O in the solution layer on stalagmite surfaces, Geochimica et Cosmochimica Acta, 73, 2592-2602, 2009.
Sinclair, D. J.: Two mathematical models of Mg and Sr partitioning into solution during incongruent calcite dissolution: implications for dripwater and speleothem studies, Chemical Geology, 283, 119-133, 2011.
Sinclair, D. J., Banner, J. L., Taylor, F. W., Partin, J., Jenson, J., Mylroie, J., Goddard, E., Quinn, T., Jocson, J., and Miklavič, B.: Magnesium and strontium systematics in tropical speleothems from the Western Pacific, Chemical Geology, 294, 1-17, 2012.
Sliwinski, J., Kost, O., Endres, L., Iglesias, M., Haghipour, N., González-Lemos, S., and Stoll, H.: Exploring soluble and colloidally transported trace elements in stalagmites: The strontium-yttrium connection, Geochimica et Cosmochimica Acta, 343, 64-83, 2023.
Stoll, H., Mendez-Vicente, A., Gonzalez-Lemos, S., Moreno, A., Cacho, I., Cheng, H., and Edwards, R. L.: Interpretation of orbital scale variability in mid-latitude speleothem δ 18 O: Significance of growth rate controlled kinetic fractionation effects, Quaternary Science Reviews, 127, 215-228, 2015.
Stoll, H. M., Müller, W., and Prieto, M.: I-STAL, a model for interpretation of Mg/Ca, Sr/Ca and Ba/Ca variations in speleothems and its forward and inverse application on seasonal to millennial scales, Geochemistry, Geophysics, Geosystems, 13, Q09004, 10.1029/2012gc004183, 2012.
Stoll, H. M., Moreno, A., Mendez-Vicente, A., Gonzalez-Lemos, S., Jimenez-Sanchez, M., Dominguez-Cuesta, M. J., Edwards, R. L., Cheng, H., and Wang, X.: Paleoclimate and growth rates of speleothems in the northwestern Iberian Peninsula over the last two glacial cycles, Quaternary Research, 80, 284-290, http://dx.doi.org/10.1016/j.yqres.2013.05.002, 2013.
Stoll, H. M., Cacho, I., Gasson, E., Sliwinski, J., Kost, O., Moreno, A., Iglesias, M., Torner, J., Perez-Mejias, C., and Haghipour, N.: Rapid northern hemisphere ice sheet melting during the penultimate deglaciation, Nature communications, 13, 1-16, 2022.
Tang, J., Köhler, S. J., and Dietzel, M.: Sr2+/Ca2+ and 44Ca/40Ca fractionation during inorganic calcite formation: I. Sr incorporation, Geochimica et Cosmochimica Acta, 72, 3718-3732, 2008a.
Tang, J., Dietzel, M., Böhm, F., Köhler, S. J., and Eisenhauer, A.: Sr2+/Ca2+ and 44Ca/40Ca fractionation during inorganic calcite formation: II. Ca isotopes, Geochimica et Cosmochimica Acta, 72, 3733-3745, 2008b.
Tesoriero, A. J. and Pankow, J. F.: Solid solution partitioning of Sr2+, Ba2+, and Cd2+ to calcite, Geochimica et Cosmochimica Acta, 60, 1053-1063, 1996.
Tremaine, D. M. and Froelich, P. N.: Speleothem trace element signatures: a hydrologic geochemical study of modern cave dripwaters and farmed calcite, Geochimica et Cosmochimica Acta, 121, 522-545, 2013.
Tzedakis, P., Drysdale, R. N., Margari, V., Skinner, L. C., Menviel, L., Rhodes, R. H., Taschetto, A. S., Hodell, D. A., Crowhurst, S. J., and Hellstrom, J. C.: Enhanced climate instability in the North Atlantic and southern Europe during the Last Interglacial, Nature communications, 9, 4235, 2018.
Wassenburg, J. A., Riechelmann, S., Schröder-Ritzrau, A., Riechelmann, D. F., Richter, D. K., Immenhauser, A., Terente, M., Constantin, S., Hachenberg, A., and Hansen, M.: Calcite Mg and Sr partition coefficients in cave environments: Implications for interpreting prior calcite precipitation in speleothems, Geochimica et Cosmochimica Acta, 269, 581-596, 2020.

Formatted: English (United States)
Formatted: English (United States)
Formatted: English (United States)